The Plant Cell, Vol. 23: 1416–1434, April 2011, www.plantcell.org

Rice APOPTOSIS INHIBITOR5 Coupled with Two DEAD-Box Adenosine 5′-Triphosphate-Dependent RNA Helicases Regulates Tapetum Degeneration [W][OA]

Xingwang Li, Xinqiang Gao, Yi Wei, Li Deng, Yidan Ouyang, Guoxing Chen, Xianghua Li, Qifa Zhang, and Changyin Wu[1]

National Key Laboratory of Crop Genetic Improvement and National Center of Plant Gene Research (Wuhan), Huazhong Agricultural University, Wuhan 430070, China

Programmed cell death (PCD) during tapetum degeneration in postmeiotic anthers is critical for the proper development of male gametophytes in flowering plants. Although several genes involved in this process have been identified recently, the molecular mechanism is still poorly understood. Here, we show that knockout of rice (*Oryza sativa*) *APOPTOSIS INHIBITOR5* (*API5*), which encodes a putative homolog of antiapoptosis protein Api5 in animals, results in delayed degeneration of the tapetum due to inhibition of the tapetal PCD process leading to defects in formation of male gametophytes. Os API5 is a nuclear protein that interacts with two DEAD-box ATP-dependent RNA helicases, API5-INTERACTING PROTEIN1 (AIP1) and AIP2. AIP1 and AIP2 are homologs of yeast (*Saccharomyces cerevisiae*) Suppressor of Bad Response to Refrigeration1 protein 2 (SUB2p) that have critical roles in transcription elongation and pre-mRNA splicing. Os AIP1 and AIP2 can form dimers and interact directly with the promoter region of *CP1*, a rice cysteine protease gene. Suppression of Os *AIP1/2* leads to down-regulation of *CP1*, resulting in sterility, which is highly similar to the effects of suppressed expression of Os *CP1*. Our results uncover a previously unknown pathway for regulating PCD during tapetum degeneration in rice, one that may be conserved among eukaryotic organisms.

INTRODUCTION

In flowering plants, male gametophyte development is essential for sexual reproduction. Male gametophytes are formed within the anther of the stamen, with a four-lobed structure, derived from anther primordial cells (Ma, 2005). After completion of anther morphogenesis, microsporocytes (also known as pollen mother cells) in each lobe are surrounded by four somatic layers: the epidermis, endothecium, middle layer, and tapetum from exterior to interior in each lobe (Goldberg et al., 1993). The development of male gametophytes depends on functional crosstalk between gametophytic and sporophytic tissues (Scott et al., 1991; Goldberg et al., 1993; McCormick, 1993; Ma, 2005). The tapetum is in direct contact with developing male gametophytes and provides the enzymes for release of microspores from tetrads and nutrients for pollen development (Goldberg et al., 1993). At the late stage of anther development, the tapetum begins to degenerate. Tapetum degeneration at the proper time is crucial for normal male gametophyte development from microspore to mature pollen grains (Pacini et al., 1985). Tapetum degradation is considered to be a process of programmed cell death (PCD; Papini et al., 1999; Wu and Cheung, 2000). Its typical cytological features, including cytoplasmic shrinkage, oligonucleosomal cleavage of DNA, vacuole rupture, and swelling of the endoplasmic reticulum, during tapetum development in angiosperms have been characterized (Papini et al., 1999; Varnier et al., 2005; Li et al., 2006). Abnormalities in tapetal degeneration usually cause male sterility in plants.

In the last decade, a number of genes regulating postmeiotic anther development have been characterized in *Arabidopsis thaliana*. *DYSFUNCTIONAL TAPETUM1* (*DYT1*), encoding a basic helix-loop-helix (bHLH) transcription factor, is required for the differentiation of tapetal cells and the formation of microspores (Zhang et al., 2006b). *DYT1* is regarded as the upstream regulator in the molecular pathway controlling postmeiotic anther development (Ma, 2005; Wilson and Zhang, 2009). *MALE STERILITY1* (*MS1*) and *ABORTED MICROSPORE* (*AMS*) were identified as the downstream genes of *DYT1* (Zhang et al., 2006b). *MS1* encodes a homolog of PHD finger transcription factors and was shown to be important for tapetal development and pollen wall formation (Ito et al., 2007; Yang et al., 2007). *AMS* encodes a bHLH protein and regulates the PCD process during tapetum development (Sorensen et al., 2003). More recently, a number of direct or downstream regulatory genes of AMS related to tapetal PCD and pollen exine formation were identified. Moreover, some interacting partners of AMS associated with anther and pollen development were also characterized (Xu et al., 2010).

With the completion of rice (*Oryza sativa*) genome sequencing and the production of libraries of tagged mutants, molecular genetic studies have also identified a few genes that influence postmeiotic anther development in rice. *UNDEVELOPED*

[1] Address correspondence to cywu@mail.hzau.edu.cn.
The author responsible for distribution of materials integral to the findings presented in this article in accordance with the policy described in the Instructions for Authors (www.plantcell.org) is: Changyin Wu (cywu@mail.hzau.edu.cn).
[W]Online version contains Web-only data.
[OA]Open Access articles can be viewed online without a subscription.
www.plantcell.org/cgi/doi/10.1105/tpc.110.082636

TAPETUM1 (*UDT1*), a putative homolog of *DYT1* in *Arabidopsis*, encodes a bHLH transcription factor and is involved in tapetal cell differentiation in rice (Jung et al., 2005). *TAPETUM DEGENERATION RETARDATION* (*TDR*), which encodes a putative bHLH transcription factor and is thought to be a putative homolog of *AMS*, acts as a downstream regulatory gene of *UDT1* and has a crucial role in tapetum degeneration and microspore development (Li et al., 2006; Zhang et al., 2008). Moreover, silencing the rice *UDP-GLUCOSE PYROPHOSPHORYLASE1* gene inhibits the degeneration of the tapetum (Chen et al., 2007). Overexpression of *Arabidopsis BI-1*, a homolog of human Bax inhibitor-1, can block tapetum PCD and cause male sterility in rice (Kawanabe et al., 2006). Recently, examinations of rice gibberellin (GA)-deficient mutants, GA-insensitive mutants, and *gamyb*, which show common defects in the PCD process during tapetum development, indicate that GA and GAMYB are required for the development of tapetum (Aya et al., 2009). Despite this progress, large efforts are still needed for understanding the detailed molecular mechanisms controlling tapetal PCD in plants.

To investigate the molecular mechanism for regulation of tapetal PCD during postmeiotic anther development in rice, we characterized a rice sterile mutant, *apoptosis inhibitor5* (*api5*), in which inhibition of the PCD process during the degeneration of tapetal cells results in complete male sterility. Os *API5* encodes a nuclear protein with a transactivation domain, regulating the PCD process by affecting the expression of a target gene, mediated by two DEAD-box ATP-dependent RNA helicases, API5-INTERACTING PROTEIN1 (AIP1) and AIP2. Highly overlapped expression patterns between *API5* and *AIP1/2* further support the interaction between API5 and AIP1/2. Finally, we demonstrated that the API5 is required for normal expression of *CP1* and that AIP1/2 directly regulates the expression of *CP1*, which might regulate tapetum degeneration during pollen development. Moreover, suppression of *AIP1/2* resulted in pollen collapse and male sterility.

RESULTS

Identification of the *api5* Mutant in Rice

To find new genes that affect the PCD process during degeneration of the rice tapetum, we identified a sterility mutant line, 03Z11RO53, from our T-DNA insertion mutant collection (Wu et al., 2003; Zhang et al., 2006a). We designated this male sterility mutant as *api5-1* because it was determined to be an *API5* knockout (see below). Genetic analyses showed that about one-quarter of T2 progenies of the heterozygous *api5-1* were sterile and others had normal fertility, indicating that the sterility was caused by a single recessive allele (fertile:sterile = 137:43; χ^2 = 0.03 for 3:1, $P < 0.01$). Relative to the wild-type plants, the *api5-1* mutant plants were normal during vegetative and floral development stages but produced smaller anthers (Figures 1A to 1D). The pollen grains of *api5-1* lacked starch, as shown by staining with iodine (Figures 1E and 1F). Pollination of the wild-type stigmas with *api5-1* pollen did not lead to seed set, indicating that male gametes were completely aborted in *api5-1*.

Delayed Degeneration of Tapetum in Anthers of *api5-1*

To determine the cause of pollen collapse in *api5-1*, we examined cross sections of anthers from the wild-type and *api5-1* mutant plants according to a recent classification consisting of 14 anther developmental stages (Zhang and Wilson, 2009). The typical anther structure with pollen mother cells surrounded by four layers of somatic cells is differentiated from the anther primordia during stages 1 to 5. Subsequently, the pollen mother cells undergo meiosis and dyads and tetrads of haploid microspores are then formed during stages 7 to 8. At stage 9, the middle layer is degenerated and almost invisible; the tapetum is more condensed, with dark staining, and has started to degenerate. Young microspores are finally released from the tetrad. No obvious differences were observed in *api5-1* anthers compared with the wild type from stages 4 to 9 (see Supplemental Figures 1A to 1H online; Figures 1G and 1H). However, the morphologic defects were observed at stage 10. At this stage, vacuolated microspores and more condensed tapetum were visible in wild-type anthers (Figure 1I), whereas in anthers of *api5-1*, the anther lobes were filled with irregular microspores and debris and the tapetum seemed slightly swollen (Figure 1J). During stage 11, the tapetum and the endothecium were completely degenerated, whereas the microspores completed mitosis in the wild type (Figure 1K). At this stage in *api5-1*, highly condensed cytoplasm and intact cell walls of tapetal cells were observed, along with fewer microspores, which had irregular shapes, and more debris and unknown particles in anther lobes (Figure 1L). At stage 12, the wild-type anther wall layer was completely degraded except for the epidermis and endothecium layer, and mature pollen grains were formed inside anther lobes (Figure 1M). However, the middle layer and belatedly degenerated tapetal cells were still visible in *api5-1* anthers, which were filled with shrunken, empty sterile microspores (Figure 1N). These observations indicate that degeneration of the tapetum is delayed in *api5-1*.

To understand better the *api5-1* anther defects, we compared anthers between the wild type and *api5-1* at the level of ultrastructure using transmission electron microscopy (TEM). Consistent with the analysis for semi-thin sections of anthers, no obvious morphological changes were observed between anthers of the wild type and *api5-1* up to stages 8 and 9 (Figures 2A to 2D). At stage 10, the tapetal cells were degenerated and it was difficult to distinguish organelles such as the nuclei and mitochondria from cellular debris in wild-type anthers (Figures 2E and 2G). However, in *api5-1* anthers, intact membrane and mitochondria were visible, while the tapetal cells were vacuolated (Figures 2F and 2H). At stage 11, most of the tapetal cells had disappeared and almost all organelles were degenerated in the remaining tapetal cells of the wild-type anthers (Figures 2I and 2K). At the same stage, the condensed cytoplasm with a surrounding membrane was detached from the tapetal cell wall in *api5-1* (Figure 2J), and within the condensed cytoplasm, intact nuclear membranes and mitochondria were also observed (Figure 2L). At stage 12, the middle layer and tapetal cells were completely degraded in the wild-type anthers (Figure 2M), and mature pollen grains were produced (Figure 2O). However, the middle layer and tapetal cells persisted in *api5-1* (Figure 2N), and highly condensed cytoplasm surrounding the obvious nuclear

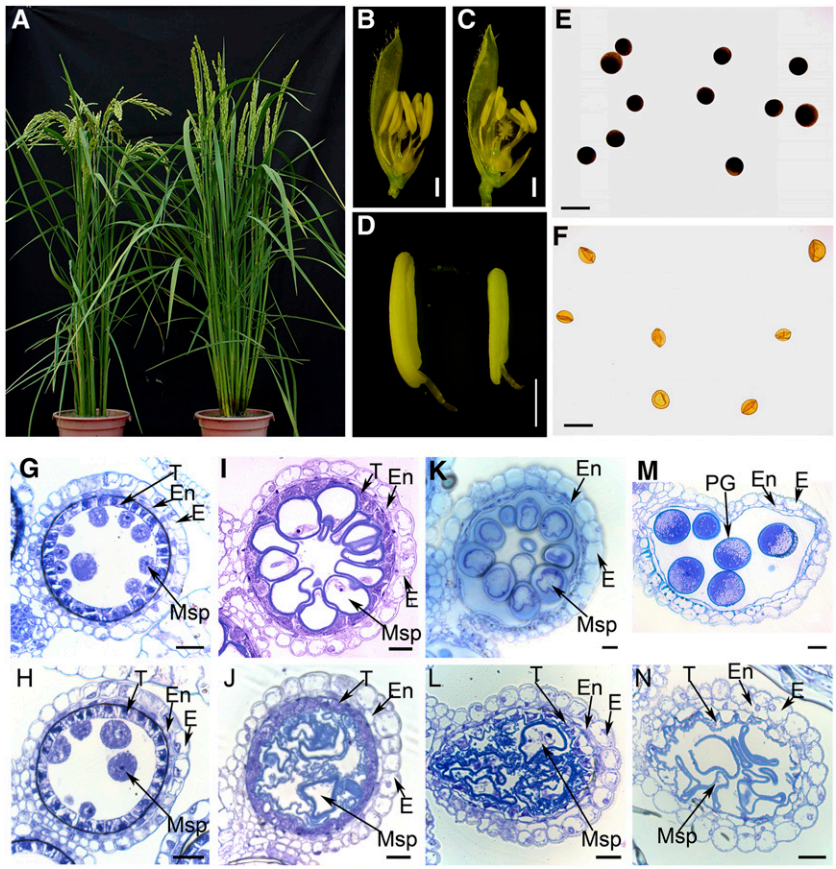

Figure 1. Comparison of the Wild Type and the *api5-1* Mutant.

(A) Phenotype comparison of the wild-type (left) and *api5-1* (right) plants after heading.
(B) and **(C)** A spikelet after removing the lemma and half of the palea from a wild-type panicle and an *api5-1* panicle, respectively.
(D) Anthers from the wild type (left) and *api5-1* (right), respectively. Bars = 1 mm in **(B)** through **(D)**.
(E) and **(F)** Pollen grain from the wild type **(E)** and *api5-1* **(F)**, respectively, stained with iodium potassium iodide solution. Bars = 30 μm.
(G) to **(N)** Cross sections of anthers from the wild type (**[G]**, **[I]**, **[K]**, and **[M]**) and *api5-1* (**[H]**, **[J]**, **[L]**, and **[N]**) at anther development stage 9 (**[G]** and **[H]**), stage 10 (**[I]** and **[J]**), stage 11 (**[K]** and **[L]**), and stage 12 (**[M]** and **[N]**). E, epidermis; En, endothecium; Msp, microspore; PG, pollen grain; T, tapetum. Bars = 25 μm.

membrane was observed in *api5-1* anthers (Figure 2P). Despite the presence of nuclear membrane, most of the organelles were degraded at this stage. However, the cells of the epidermis in *api5-1* anthers were expanded. Although the middle layer and tapetum developed abnormally in *api5-1* anthers, orbicules and the cuticle of the outer epidermis cell wall seemed normally formed (Figures 2M and 2N). Furthermore, pollen wall development was not affected in *api5-1* compared with the wild-type anthers during stages 8 to 12 (see Supplemental Figures 2A to 2J online). These observations suggest that delayed degeneration of the tapetum occurs in *api5-1*, but that pollen wall development and orbicule formation are not affected.

Tapetal PCD Is Inhibited in *api5-1*

The degeneration of the tapetum in anthers is considered to result from PCD, with fragmentation of nuclear DNA as a typical feature (Li et al., 2006). To compare the PCD process in anthers between the wild type and *api5-1*, terminal deoxynucleotidyl transferase-mediated dUTP nick-end labeling (TUNEL) assays were performed with anthers at different developmental stages. At the early part of stage 8, TUNEL-positive signals in nuclei of tapetal cells were undetectable in both the wild type and *api5-1*, indicating that DNA fragmentation had not occurred at this stage (Figures 3A and 3B). TUNEL signals were clearly detected in the tapetal cells of the wild type, but were lacking in *api5-1* at the tetrad stage (Figures 3C and 3D), suggesting that tapetal PCD was repressed in the *api5-1* mutant. Subsequently, the wild-type anthers showed strong TUNEL-positive signals in tapetal cells and vascular bundles at stage 9, but TUNEL signals were also observed in the outer cell layers of the anther (endothecium and middle layer) and vascular bundle cells (Figure 3E). Compared with the wild type, a lower level of TUNEL signal was detected in the *api5-1* tapetum (Figure 3F). At stage 10, intensely TUNEL-positive nuclei were present in degenerating tapetum in the wild type (Figure 3G), and a strong signal was also observed in the

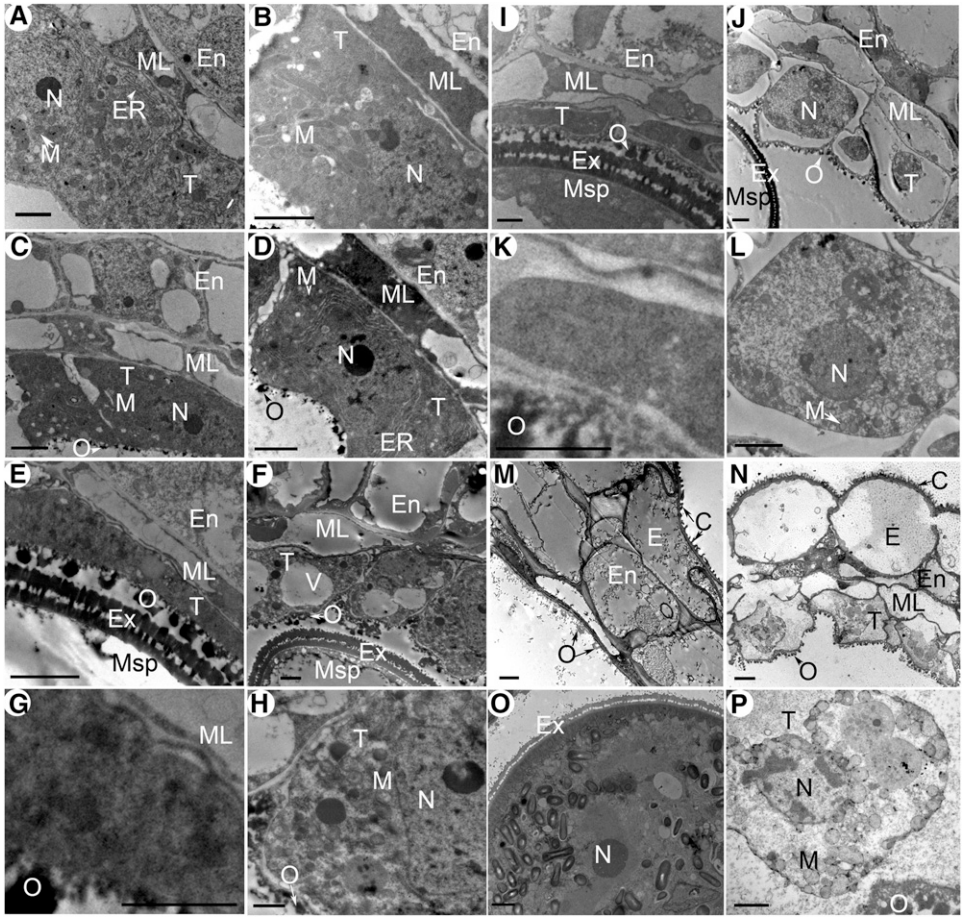

Figure 2. TEM Analyses of Anthers in the Wild Type and *api5-1*.

(A) to **(F)** Cross sections of the wild-type (**[A]**, **[C]**, and **[E]**) and *api5-1* (**[B]**, **[D]**, and **[F]**) anthers at late stage 8 (**[A]** and **[B]**), stage 9 (**[C]** and **[D]**), and stage 10 (**[E]** and **[F]**).

(G) and **(H)** Magnified view of tapetum region in **(E)** and **(F)**, respectively.

(I) and **(J)** Cross sections of the wild-type **(I)** and *api5-1* **(J)** anthers at stage 11.

(K) and **(L)** Magnified view of tapetum region in **(I)** and **(J)**, respectively.

(M) and **(N)** Cross sections of the wild-type **(M)** and *api5-1* **(N)** anthers at stage 12.

(O) Cross sections of the wild-type pollen grains.

(P) Magnified view of tapetum region in **(N)**.

C, cuticle; E, epidermis; En, endothecium; ER, endoplasmic reticulum; Ex, exine; M, mitochondria; ML, middle layer; Msp, microspores; N, nucleus; O, orbicule; T, tapetal cell; V, vacuole. Bars = 2 μm in **(A)** to **(F)**, **(I)**, **(J)**, and **(M)** to **(O)**, and 1 μm in **(G)**, **(H)**, **(K)**, **(L)**, and **(P)**.

tapetal cells of *api5-1* anthers (Figure 3H). No obvious difference in DNA fragmentation in sporophytic cells, including the epidermis and vascular bundles, was observed between the wild type and *api5-1* (Figures 3G and 3H). These findings indicate that PCD, which was inhibited in the tapetum, was taking place normally elsewhere in *api5-1* anthers.

We further quantitatively characterized the extent of DNA fragmentation in the wild type and *api5-1* mutant anthers using comet assays (Li et al., 2006; Wang and Liu, 2006). At early stage 8, *api5-1* mutant anthers exhibited a slightly lower level of DNA damage compared with that in the wild type. From late stage 8 to stage 10, DNA damage was obviously increased in the wild type. However, the *api5-1* mutant anthers showed a lower level of DNA damage than the wild type during those stages (Figure 3I). These results substantiated the idea that the lessened extent of PCD caused the delayed degeneration of tapetum in the *api5-1* anthers.

Disruption of *API5* Caused Male Sterility

The genomic sequence flanking the T-DNA insertion site in the *api5-1* mutant was isolated, and a BLASTn search of the T-DNA flanking sequence against the genomic sequence database (http://rice.plantbiology.msu.edu) showed that the T-DNA was inserted into the last exon of a predicted gene located on chromosome 2 (Figure 4A), which was annotated as *API5* in

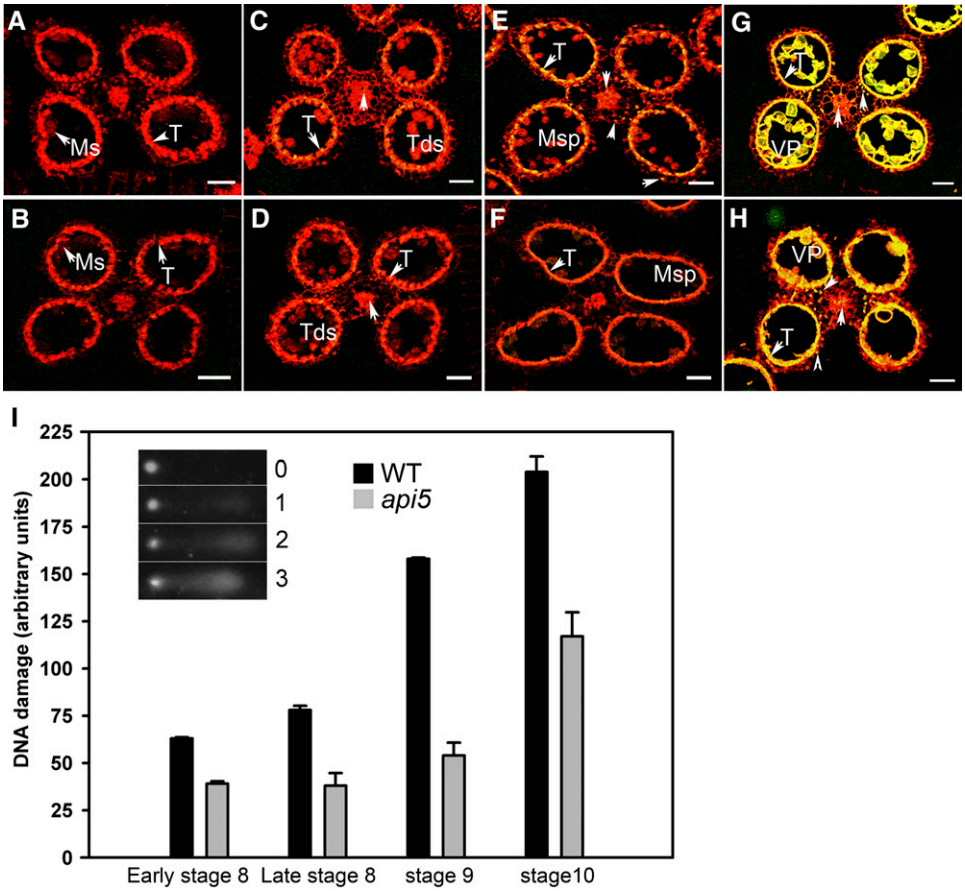

Figure 3. Comparison of DNA Fragmentation in the Anthers of the Wild Type and *api5-1*.

(A) to **(H)** DNA fragmentation in anthers of the wild type (**[A]**, **[C]**, **[E]**, and **[G]**) and *api5-1* (**[B]**, **[D]**, **[F]**, and **[H]**) at early stage 8 (**[A]** and **[B]**), late stage 8 (**[C]** and **[D]**), stage 9 (**[E]** and **[F]**), and stage 10 (**[G]** and **[H]**) as assayed using the TUNEL method. The red fluorescence indicates nuclei stained with propidium iodide, and the yellow fluorescence is TUNEL-positive signal arising from the red fluorescence of background staining merged with the green fluorescence of TUNEL-positive nuclei staining. Arrows without labels indicate TUNEL-positive signals in connective tissue and epidermis of anther. Ms, microsporocyte; Msp, microspore; T, tapetum; Tds, tetrads; VP, vacuolated pollen. Bars = 50 μm.

(I) Quantitative comparison of DNA fragmentation in the wild-type (WT) and *api5-1* anthers at early stage 8, late stage 8, stage 9, and stage 10 was performed using comet assays. The extent of DNA damage in each nucleus is quantified using the units 0, 1, 2, or 3. An increased unit correlated with a higher DNA percentage in the tail, as shown in the demonstration gel in the upper left corner of the graph. Values shown in the graph are obtained by summing the units from 100 nuclei on each slide + SE of three independent experiments.

rice. Genotyping of T1 plants showed that the T-DNA insertion of *api5-1* cosegregated with the sterile phenotype (see Supplemental Figure 3A online). Another T-DNA insertion line, 3A-10121 (this line is designated as *api5-2*), in which the T-DNA insertion site was located in the 13th exon of *API5* (Figure 4A), showed the same complete male-sterile phenotype as that in the *api5-1* mutant (see Supplemental Figures 4A to 4H online), and the T-DNA insertion of *api5-2* cosegregated with the sterile phenotype, as in the case of *api5-1* (see Supplemental Figure 3B online). RT-PCR analysis revealed that the *API5* transcript was not detectable in *api5-1* or *api5-2* (Figure 4B). These data indicate that the T-DNA insertions are knockout mutations of *API5*, resulting in male sterility.

To confirm that the sterility is caused by the loss of function of *API5*, a 15.1-kb genomic fragment containing the entire Os *API5* coding region was introduced into callus prepared from a homozygous T-DNA insertion line of *api5-1* (see Supplemental Figure 3C online). Of 51 independent transgenic plants generated, 39 showed restored fertility (see Supplemental Figure 3D online), whereas 12 plants transformed with empty vector (negative control) retained a sterile phenotype similar to that of *api5*. In the progenies of the rescued plants with a single copy of the transgene, segregation of the *API5* transgene coincided very well with normal fertility (see Supplemental Figures 3E and 3K online). All positive transgenic plants showed normal fertility, anthers, and starch-filled pollen grains, while negative transgenic plants produced smaller anthers and collapsed pollen (see Supplemental Figures 3F to 3J online). Therefore, we concluded that loss of function of *API5* was the cause of the male sterility in *api5*.

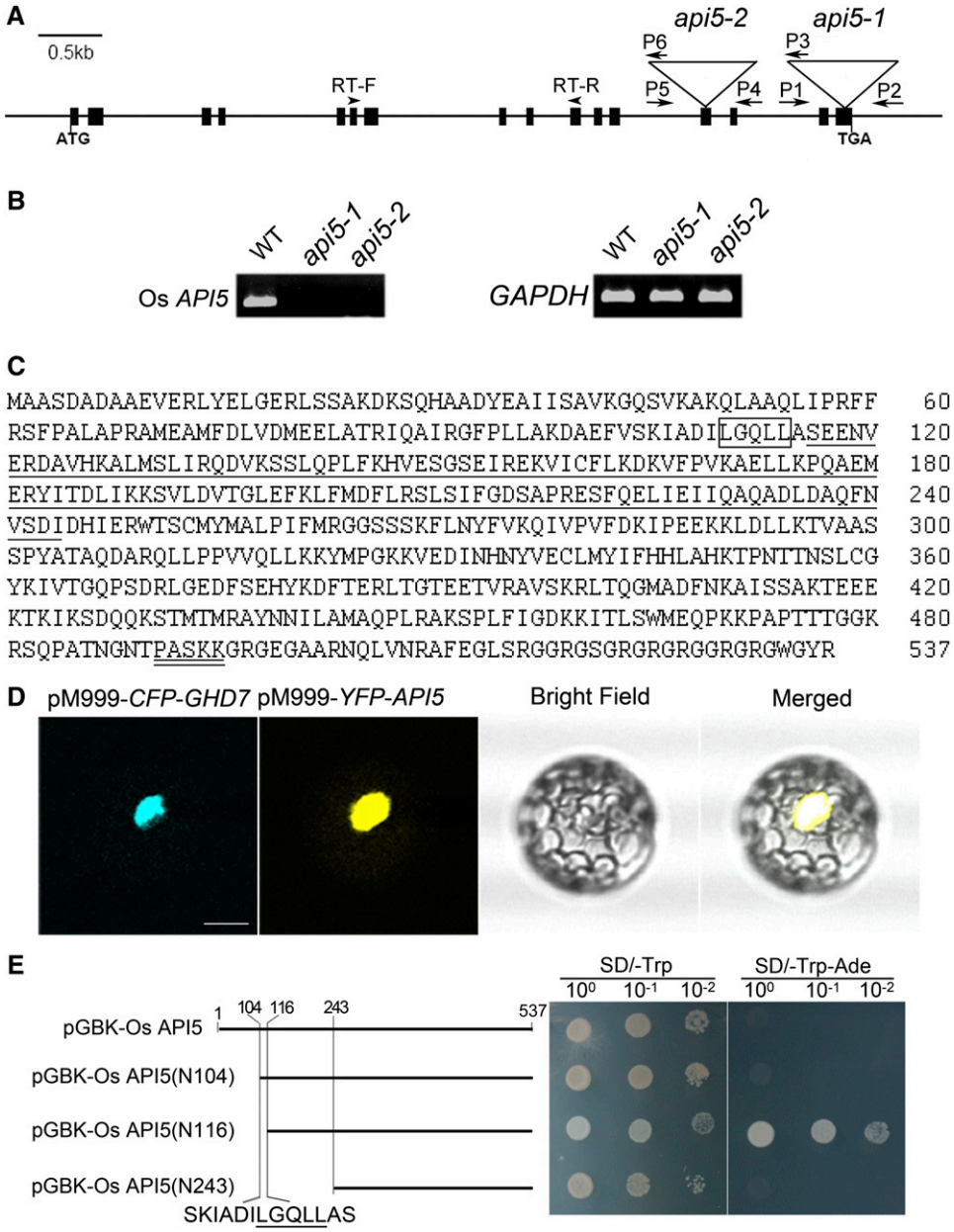

Figure 4. Molecular Identification of Os *API5*.

(A) Structure of *API5* and T-DNA insertion sites. Filled boxes represent exons and lines represent introns; T-DNA insertion sites are located in exons 16 and 13 in *api5-1* and *api5-2*, respectively. P1 to P6 indicate the PCR primers used for genotyping the T-DNA in *api5-1* and *api5-2*. RT-F and RT-R indicate the RT-PCR primers for analyzing *API5* expression.

(B) RT-PCR analyses of *API5* expression levels in the wild type (WT), *api5-1*, and *api5-2*. Total RNA was extracted from spikelets of stage 8/stage 9. *GAPDH* was used as a control.

(C) Amino acid sequence of API5 protein. The LXXLL motif is boxed. The nuclear localization signal is double underlined. The transactivation domain is underlined.

(D) Subcellular localization of full-length Os API5 fused with yellow fluorescent protein (YFP); a nuclear protein, GHD7-fused cyan fluorescent protein (CFP), was used as a nuclear marker (leftmost image). The two proteins were coexpressed in *Arabidopsis* protoplasts. A bright-field image and the merged image are shown on the right. Bar = 10 μm.

(E) Schematic representations of full-length and a series of truncated Os API5 fusions to DNA binding domain (BD), and transcriptional activation activity assays of the indicated proteins. The numbers indicate the amino acid position relative to the N terminus of API5. The growth of transformants on SD/−Trp−Ade medium indicates the corresponding protein possesses transcriptional activation activity. The polypeptide sequence (SKIADILGQLLAS) between positions 104 to 116 of Os API5 is shown at the bottom.

Characterization of *API5* in Rice

Os *API5* encodes a homolog of animal API5, with 537 amino acids, including a nuclear localization signal, a LXXLL motif, and a transcription activation domain (Figure 4C). To test the functions of these domains, we examined the subcellular localization of Os API5. The YFP-fused full-length Os API5 was colocalized with CFP-fused GHD7 (Xue et al., 2008) in *Arabidopsis* protoplasts (Figure 4D), suggesting that Os API5 is also a nuclear protein.

We next investigated the transcriptional activation activity of Os API5 in yeast (*Saccharomyces cerevisiae*). No transcriptional activation of Os API5 was detected when the yeast strain was transformed with GAL4 DNA BD fused with full-length Os API5. Serial deletions of Os API5 from the N-terminal region to 243 amino acids were assayed to test their transcriptional activity. A truncated Os API5 protein, with a deletion of 12 amino acids encompassing the LXXLL motif, resulted in activation of transcription (Figure 4E). These results suggest that a functional transcription activation domain might exist in Os API5 and that the LXXLL motif is a likely suppressor of the transcription activation.

Quantitative RT (qRT)-PCR analysis revealed that *API5* is expressed in all tissues analyzed, including root, leaf blades, leaf sheath, culms, and panicles (Figure 5A). Unexpectedly, it was expressed more highly in roots than in panicles. To determine the precise expression pattern of *API5*, RNA in situ hybridization was performed in sections of anthers from late stages 8 to 10, as well as in vegetative tissues. *API5* transcripts were detected in the parietal anther wall layers and microsporocyte, with stronger signal in tapetum in all the examined stages (Figures 5B to 5D). In vegetative tissues, transcripts of *API5* were detected in epidermal cells in roots (Figures 5F and 5G), vascular tissues in culms (Figure 5I), and mesophyll cells in leaf blades (Figure 5J). As expected, sense probe used as a negative control gave rise to only a faint, almost undetectable, signal (Figures 5E, 5H, and 5K). The preferential expression of *API5* in the tapetum is consistent with its inferred function in the differentiation of the tapetum during anther development. The expression of *API5* in vegetative tissues suggests that it has other functions in growth and development that may be complemented by other gene product(s) in the *api5* mutant.

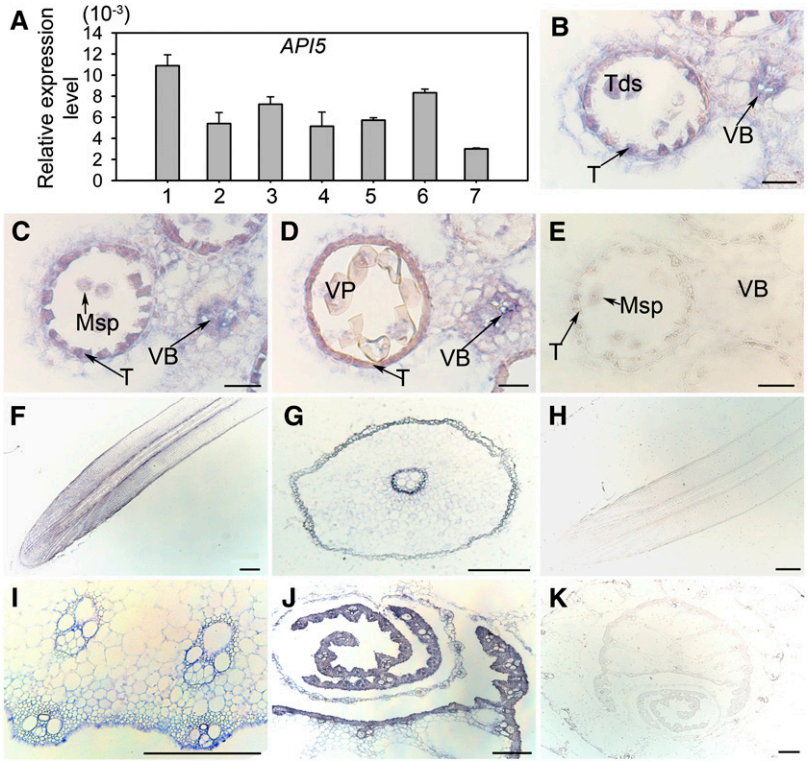

Figure 5. Expression Pattern of Os *API5*.

(A) qRT-PCR analysis of *API5* expression levels in 4-week-old roots (1), culms (2), leaves (3), sheathes (4), and panicles of 4 cm (5), 10 cm (6), and 16 cm (7) in length, respectively. *Ubiquitin5* was used as a control for normalization. The data shown are the means ± SE of three independent experiments.
(B) to **(D)** In situ hybridization assays of *API5* in anthers at late stage 8 **(B)**, stage 9 **(C)**, and stage 10 **(D)**.
(E) Negative controls with sense probe in anthers at late stage 9.
(F), **(G)**, **(I)**, and **(J)** In situ hybridization assays of *API5* in longitudinal section of root **(F)**, transverse section of root **(G)**, transverse section of culm **(I)**, and transverse section of leaf **(J)**.
(H) and **(K)** Negative controls with sense probe in longitudinal section of root **(H)** and transverse section of leaf **(K)**. The samples of root and leaf were collected from 4-week-old seedlings, and the culm from 8-week-old seedlings. Bars = 20 μm in **(B)** through **(E)** and 200 μm in **(F)** through **(K)**.
Msp, microspore; T, tapetum; Tds, tetrads; VB, vascular bundle; VP, vacuolated pollen.

Os API5 Belongs to an Ancient Family That Is Conserved among Eukaryotes

API5 proteins exist in the majority of eukaryotes (Morris et al., 2006). To learn more about functions of *API5* in different organisms, we constructed a phylogenetic tree using API5 homologs from protists, plants, and animals. Since most of the species, including rice, contained only one member of the API5 family, only one API5 protein of a species was used for alignment and analysis to avoid over-representation from certain species (see Supplemental Data Set 1 online). In this way, 32 API5 protein sequences were classified into three clusters according to the phylogenetic tree (Figure 6). This result of clustering was consistent with major taxonomic groupings of animals, plants, and protists. The three major groups in the phylogenetic analyses may indeed reflect the systematization of animals, plants, and protists.

Overexpression of *API5* in Rice

To gain more knowledge regarding the function of *API5*, we developed transgenic lines harboring the full-length coding sequence (CDS) of Os *API5* driven by the maize *Ubiquitin* promoter in the genetic background of japonica cultivar Zhonghua11. The relative expression level of *API5* between transgene-positive and -negative plants of the T1 generation derived from a single copy

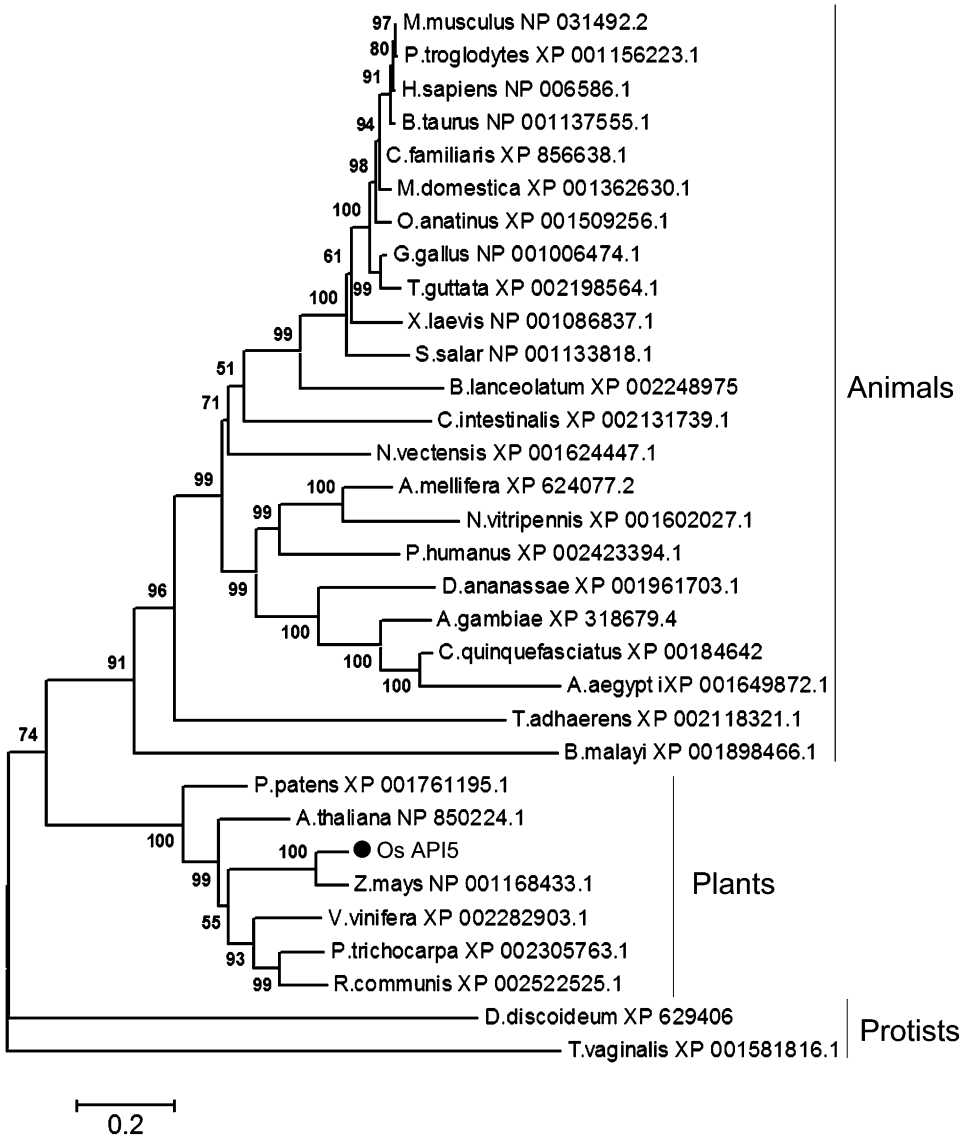

Figure 6. A Phylogenetic Tree of the API5 Family Proteins.

Phylogenetic analysis was conducted using MEGA 3.1. Thirty-two API5 homologs were selected for establishing a bootstrap N-J phylogenetic tree and 1000 replicates were conducted to determine the statistical support for each node. The black dot shows the position of Os API5. A text file of the alignment used to generate this tree is available as Supplemental Data Set 1 online.

transgenic T0 plant was verified by qRT-PCR. The amount of *API5* transcripts in positive plants was significantly enhanced (>80-fold) compared with negative plants (see Supplemental Figure 5A online). The normal fertility of both positive and negative plants suggested that the development of reproductive organs was normal in *API5*-overexpressing plants (see Supplemental Figure 5B online). We also examined the morphology of the positive plants relative to their negative counterparts at the seedling and reproductive stages, and also the cytologic characteristics of roots, culms, and leaves (see Supplemental Figures 5C to 5F, 5H, 5I, 5L, 5N, and 5O online). No obvious differences were observed between them. We also compared cross sections of these vegetative tissues in *api5-1* and did not observe any visible changes (see Supplemental Figures 5G, 5J, 5M, and 5P online). These results indicated that overexpression or knockout of *API5* did not affect the vegetative growth in rice under normal growth conditions.

API5 Physically Interacts with AIP1 and AIP2

Previous studies identified the human Api5 protein (FIF/AAC-11) as an interacting factor of FGF-2 and Acinus (Van den Berghe et al., 2000; Rigou et al., 2009). To find interacting proteins for Os API5, we searched the rice protein database (NCBI) with FGF-2 and Acinus proteins and found no obvious homologs of FGF-2 or Acinus. We then hypothesized that API5 might interact with other proteins in rice to regulate the degeneration of tapetal cells. To identify the potential partners of API5, full-length Os API5 was used as a bait to screen a prey cDNA library prepared from panicles of rice using the yeast two-hybrid method. Two putative DEAD-box ATP-dependent RNA helicases, which were designated AIP1 and AIP2, respectively, were confirmed to interact physically with API5 (Figure 7A). Both *AIP1* and *AIP2* were predicted to encode proteins with 432 amino acids, and they are identical except for three amino acids, which do not interfere with the interaction between API5 and AIP1/2.

We used AIP1 for confirmation of the interaction with API5. A BiFC assay (Walter et al., 2004) using *Arabidopsis* protoplasts demonstrated that the two proteins indeed interacted with each other and that both of the interacting proteins had a nuclear localization (Figure 7B). In vitro interaction between these two proteins was further assayed using coimmunoprecipitation (Co-IP). The results indicated that API5 interacts with AIP1 directly in vitro (Figure 7C). All of these data provide solid evidence of the physical interaction between Os API5 and Os AIP1.

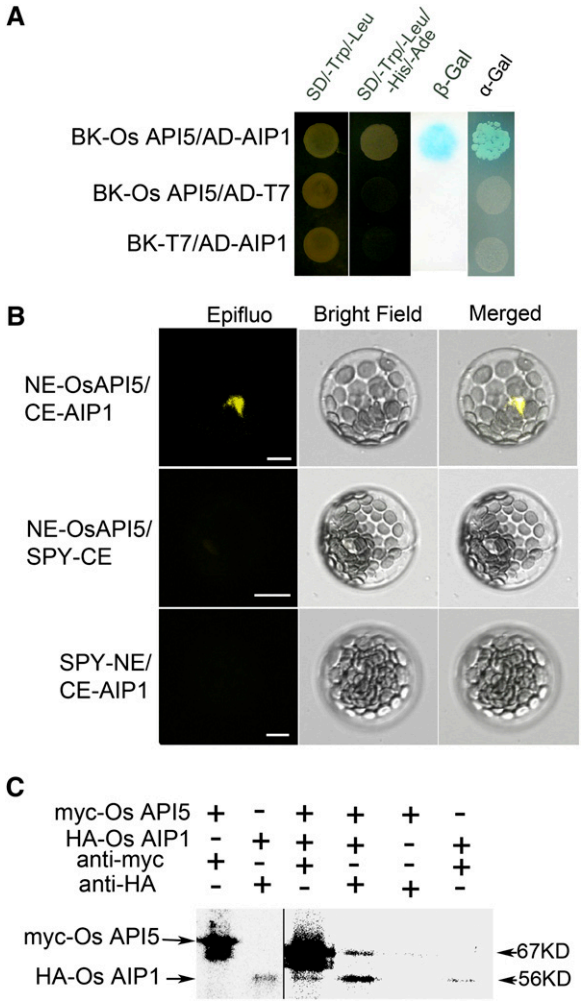

Figure 7. Interaction of Os API5 with Os AIP1 in Vivo and in Vitro.

(A) Os API5 interacts with the Os AIP1 in yeast two-hybrid assays. The empty pGBK-T7 and pGAD-T7 vectors were used as negative controls. The blue colonies on selective medium SD/−Trp−Leu−His−Ade indicate the positive interaction.

(B) Bimolecular fluorescence complementation (BiFC) assays of Os API5 interaction with Os AIP1 in vivo. The yellow fluorescence signal indicates the positive interaction. The expression of Os API5 or Os AIP1 alone (NE-Os API5/ SPY-CE and SPY-NE/ CE-Os AIP1) was used as negative control.

(C) Interaction between c-*myc* fused Os API5 and HA-fused Os AIP1 was verified by Co-IP assays in vitro.

Knockdown of Both *AIP1* and *AIP2* Results in Low Fertility

To test whether *AIP1* and *AIP2* are involved in regulating the degeneration of tapetum in rice, we generated transgenic plants suppressing the expression of *AIP1* and *AIP2* simultaneously using an overexpressed artificial micro-RNA (*amiRNA-AIP1/2*), which specifically targets a homologous region in the 3′ untranslated region of *AIP1* and *AIP2* mRNAs (Figure 8A). Eighty-six independent *amiRNA-AIP1/2* transgenic plants were generated, and 31 plants showed low fertility (seed setting rate <20%, including 16 completely sterile plants). Two *amiRNA-AIP1/2* transgenic plants (S81 and S82) showing complete sterility were selected for further characterization. Coinciding with elevated expression of *amiRNA-AIP1/2*, expression of *AIP1/2* decreased in the transgenic plants (Figures 8B and 8C).

To examine the effects of *AIP1/2* on anther development, we also checked the cross sections of anthers of line S81 from stages 9 to 12. At stage 9, no obvious differences were observed in microspores or anther wall layers between S81 and transgenic-negative plants (Figures 8D and 8E). However, at stages 10 and 11, just as in *api5-1* anthers, persistent tapetal cells with condensed cytoplasm and irregularly shaped microspores were

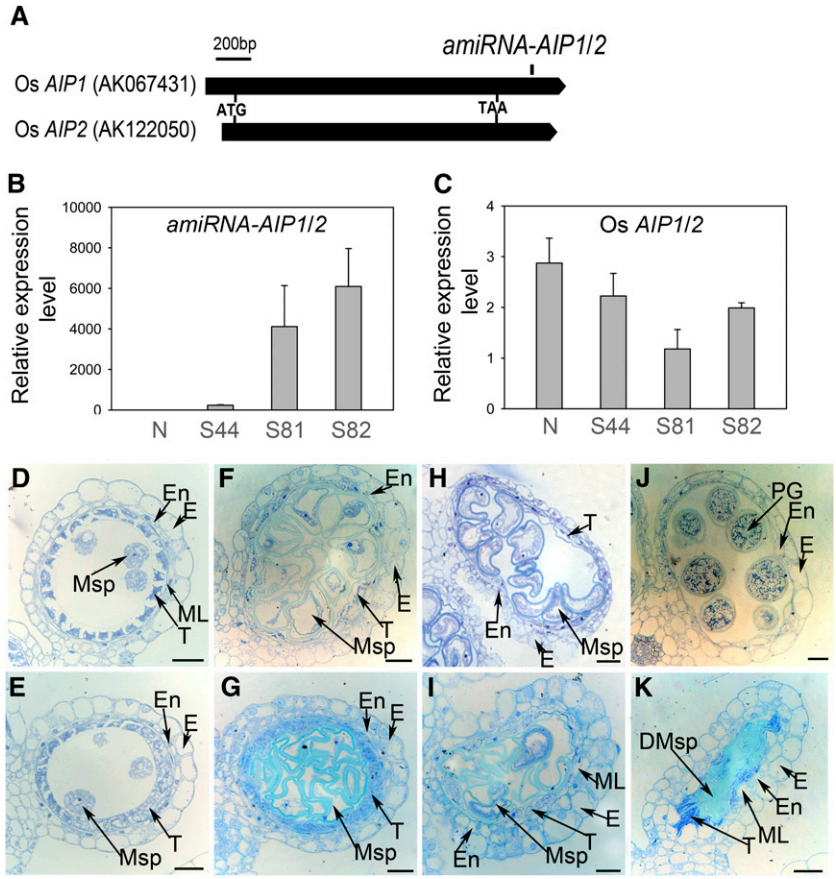

Figure 8. Characterization of Os *AIP1/2*-Suppressed Plants.

(A) Schematic diagram of *amiRNA-AIP1/2* location in full-length cDNA of *AIP1* and *AIP2*.
(B) and **(C)** The transcript levels of mature *amiR-AIP1/2* **(B)** and *AIP1/2* **(C)** in *amiR-AIP1/2* transgenic plants. N, transgene-negative plant; S44, S81, and S82 are transgene-positive plants. Total RNA was extracted from the spikelet of the stage 8/stage 9 of the plant. Rice *Ubiquitin5* was used as an internal control. The data shown are the means ± SEM of three independent experiments.
(D) to **(K)** Cross sections of anthers of the wild type (**[D]**, **[F]**, **[H]**, and **[J]**) and line S81 (**[E]**, **[G]**, **[I]**, and **[K]**) from stage 9 (**[D]** and **[E]**), stage 10 (**[F]** and **[G]**), stage 11 (**[H]** and **[I]**), and stage 12 (**[J]** and **[K]**). DMsp, degenerated microspore; E, epidermis; En, endothecium; ML, middle layer; Msp, microspore; PG, pollen grain; T, tapetum. Bars = 20 μm.

observed in S81 (Figures 8G and 8I) compared with the wild type (Figures 8F and 8G). Subsequently, microspores were completely collapsed and the tapetum was retained in the anthers of S81 at stage 12 (Figure 8K). Thus, like *API5*, *AIP1* and *AIP2* are required for tapetal degradation and pollen development.

Expression Profile of Os *AIP1/2*

It was difficult to design RT-PCR primers to examine the expression patterns of *AIP1* and *AIP2* separately because of the high similarity between their CDSs. qRT-PCR analysis revealed that *AIP1/2* was constitutively expressed in root, shoot, leaf, sheath, and panicles of different developmental stages (Figure 9A). The expression levels of *AIP1/2* were not altered in *api5-1* compared with the wild type (see Supplemental Figure 6A online), indicating that the expression of *AIP1/2* is likely independent of *API5* in rice.

RNA in situ hybridization was performed for further detection of *AIP1/2* transcripts in anthers from late stage 8 to stage 10 and in vegetative tissues (roots, culms, and leaves). Similar to the expression patterns of *API5*, intensive signals for *AIP1/2* were visible in tapetal cells and vascular bundles of connective tissues in anthers at different developmental stages (Figures 9B to 9D). *AIP1/2* transcripts were also detected in root pericycle cells, vascular bundles, and epidermis cells in culms and leaves (Figures 9F to 9H), but not in the negative controls (Figures 9E and 9I). Such coinciding expression patterns for *API5* and *AIP1/2* further support that they exert their function in tapetum degeneration through the formation of a API5-AIP1/2 complex.

Subcellular Localization and Dimerization of AIP1/2

Both *AIP1* and *AIP2* encode putative DEAD-box ATP-dependent RNA helicases that contain two highly conserved domains,

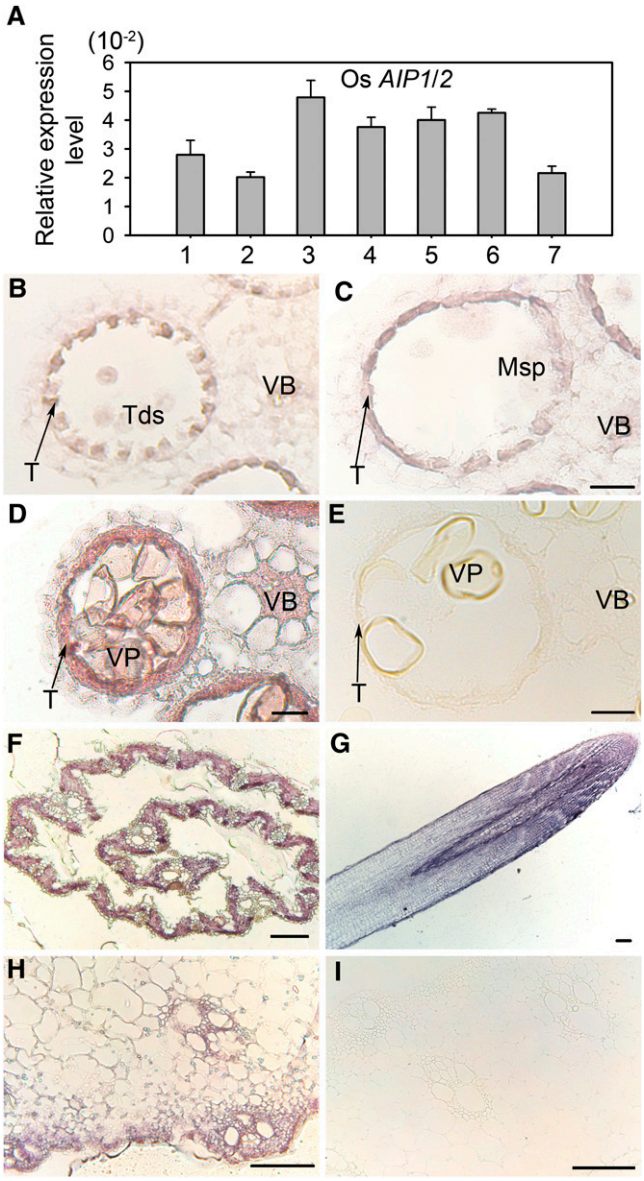

Figure 9. Expression Pattern of Os *AIP1/2*.

(A) qRT-PCR analysis of *AIP1/2* expression levels in 4-week-old roots (1), culms (2), leaves (3), sheathes (4), and panicles of 4 cm (5), 10 cm (6), and 16 cm (7), respectively. *Ubiquitin5* was used as a control. The data shown are the means ± SE of three independent experiments.

(B) to **(D)** In situ hybridization assay of *AIP1/2* in anthers at late stage 8 **(B)**, stage 9 **(C)**, and stage 10 **(D)**, and in leaf **(F)**, root **(G)** and culm **(H)**.

(E) and **(I)** Negative controls with sense probe in anthers at late stage 10 **(E)** and transverse section of culm **(I)**. Bars = 20 μm in **(B)** to **(E)** and 100 μm in **(F)** to **(I)**.

Msp, microspore; T, tapetum; Tds, tetrads; VB, vascular bundle; VP, vacuolated pollen.

DEAD/H-box helicase (PF00270) and helicase-conserved C-terminal domain (PF00271; Figure 10A). In the previous sections, we showed that Os API5 and Os API5-Os AIP1 complexes were localized in the nuclei of *Arabidopsis* protoplasts. Next, we individually examined the subcellular localization of Os AIP1 and Os AIP2. The full-length Os AIP1-fused YFP and the empty construct pM999-GFP (green fluorescent protein) were co-transformed into *Arabidopsis* protoplasts. The signals of YFP and GFP overlapped in the cytoplasm and nuclei of protoplasts (Figure 10B). In addition, the same distribution pattern in the protoplasts of Os AIP2 with GFP of the empty construct pM999-GFP was also observed (see Supplemental Figure 6B online). These results indicated that Os AIP1 and Os AIP2 may be distributed in the nucleus and cytoplasm, and localized in nuclei exclusively after formation of the API5-AIP1/2 complex.

Tanner and Linder (2001) reported that the formation of dimers was required for RNA helicase activity in many associated biological processes. To test this possibility, a yeast two-hybrid assay was conducted to investigate the interaction between AIP1 and AIP2. As shown in Figure 10C, AIP1 can form a homodimer in yeast. In addition, formation of the homodimer of AIP2 and heterodimers of AIP1 and AIP2 were also observed in yeast (see Supplemental Figure 6C online). In vivo dimerization of AIP1 was further confirmed in BiFC assays (Figure 10E). Taken together, we speculated that AIP1 and AIP2 may interact with API5 to regulate PCD.

Os AIP1 and Os AIP2 Can Complement the Yeast *sub2* Mutant

A BLASTp search of Os AIP1/2 against the NCBI reference protein database (http://blast.ncbi.nlm.nih.gov/) showed that Os AIP1/2 had 76% and 72% identity with human UAP56 (hUAP56) and yeast Suppressor of Bad Response to Refrigeration1 protein 2 (SUB2p; Figure 10D), respectively. In addition, Os AIP1 and Os AIP2 possess all seven highly conserved motifs characterized in hUAP56 and SUB2p (Figure 10D). These analyses indicated that Os AIP1 and Os AIP2 may be putative homologs of hUAP56 and SUB2p. To confirm this hypothesis, Os AIP1 and Os AIP2 were used to rescue the lethal phenotype of yeast *sub2* mutant. The diploid yeast strain BY4743 that was heterozygous for the *SUB2* locus, in which the allelic *SUB2* was replaced by a Genetin (G418) resistance gene, was transformed with pGAD-AIP1 or pGAD-AIP2. The transformants were able to grow on synthetic dropout Leu medium (SD/−Leu), because a Leu selection marker was contained in both pGAD-AIP1 and pGAD-AIP2 plasmids, and a clone was then selected for sporulation, producing two kinds of haploid progeny with different genotypes (*MATa*, *his3Δ1*, *leu2Δ0*, *lys2Δ0*, *MET15*, *ura3Δ0*, *sub2*::*G418*, Os AIP1/2, Leu and *MATα*, *his3Δ1*, *leu2Δ0*, *LYS2*, *met15Δ0*, *ura3Δ0*, *SUB2*, Os AIP1/2, Leu). If Os AIP1or Os AIP2 could functionally complement the yeast *sub2* mutant, the G418-resistant *sub2*::*G418/AIPs* haploids and G418-sensitive *SUB2/AIPs* haploids would grow on synthetic dropout medium (SD/−Met/G418) but not on SD/−Lys/G418 medium (Figure 10F). No haploids were produced in the negative controls on the same medium (nontransformed or pGAD-T7 empty vector-transformed BY4743). As expected, both pGAD-AIP1 and pGAD-AIP2 rescued the yeast *sub2* mutant. The

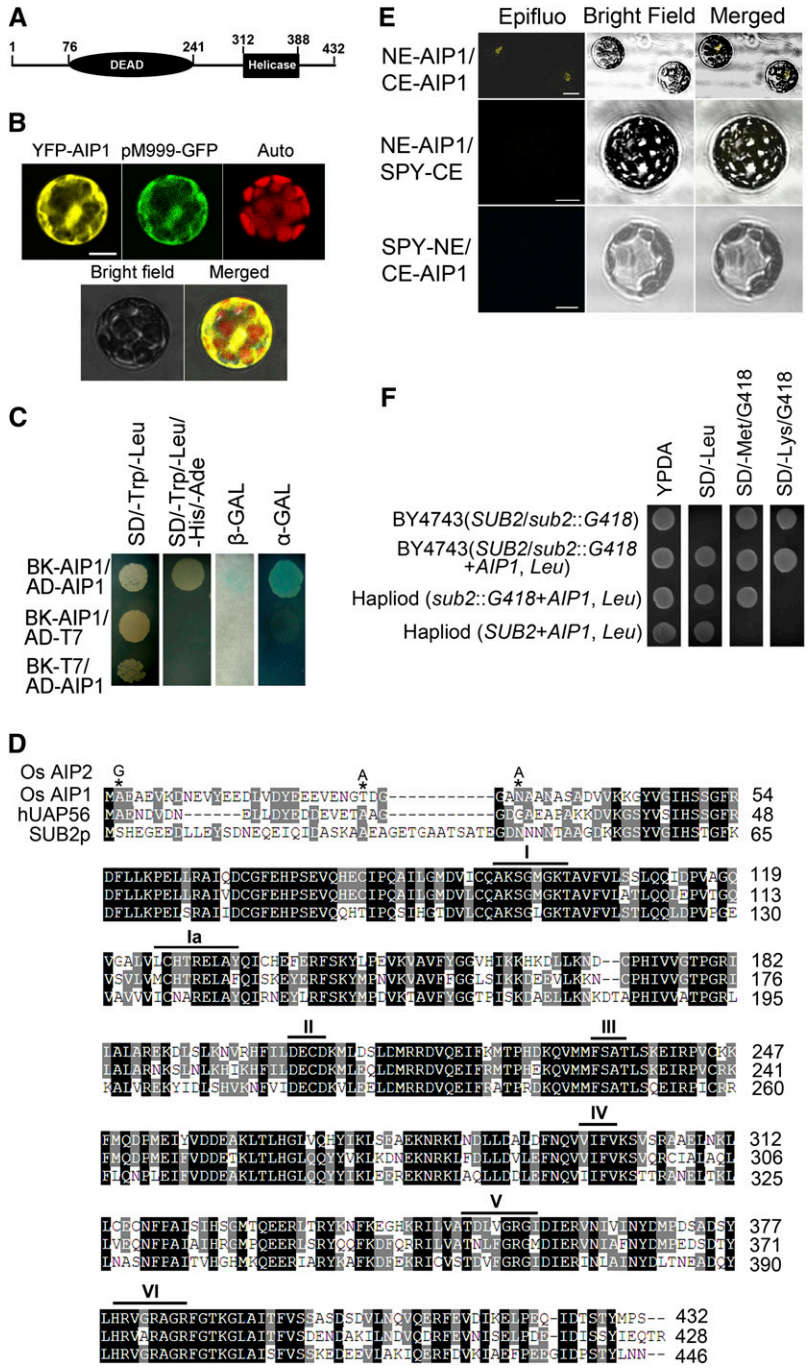

Figure 10. Features of Os AIP1/2.

(A) Domain organization of Os AIP1 and Os AIP2. The numbers indicate amino acid positions.

(B) Subcellular localization of Os AIP1 fused with YFP; an empty vector containing the GFP reporter gene (pM999-GFP) was used as a marker. Chlorophyll autofluorescence (Auto) is shown, as are bright-field and merged images. Bar = 10 μm.

(C) Os AIP1 homodimers were detected in yeast two-hybrid assays. The blue colonies on selective medium SD/−Trp−Leu−His−Ade indicate the positive interaction. The empty pGBK-T7 (BK-T7) and pGAD-T7 (AD-T7) vectors were used as negative controls.

(D) Alignment of Os AIP1, Os AIP2, hUAP56, and SUB2p. Black boxes highlight identical amino acids, and gray boxes highlight similar residues. Thick black bars above the aligned sequences highlight the seven conserved motifs (I, Ia, and II to VI). Amino acids with asterisks indicate the three different amino acids between Os AIP1 and Os AIP2.

(E) Os AIP1 dimerization was observed in BiFC assays. The yellow fluorescence signal indicates the positive interaction. The expression of Os AIP1 alone (NE-AIP1/SPYCE and SPYNE/CE-AIP1) was used for negative controls. Bars = 10 μm.

(F) Complementation of the yeast *sub2* mutant with Os AIP1/2. The growth of BY4743 (*MATa*/α, *his3Δ1*/*his3Δ1*, *leu2Δ0*/*leu2Δ0*, *lys2Δ0*/*LYS2*, *MET15*/*met15Δ0*, *ura3Δ0*/*ura3Δ0*, *sub2*::*G418*/*SUB2*) and transformants in different mediums; *MET15* and *LYS2* were used for selection of haploids. The transformants with G418 resistance can grow in selective medium lacking Leu and Met, indicating AIP1/2 could rescue the yeast *sub2* mutant.

genotype of G418-resistant *sub2*::*G418*/*AIPs* haploids and G418-sensitive *SUB2*/*AIPs* haploids were further confirmed on SD/−Met and SD/−Lys medium (Figure 10F). We conclude that Os AIP1 and Os AIP2 are the functional homologs of yeast SUB2p.

AIP1/2 Directly Regulates the Expression of *CP1*

To find putative downstream genes regulated by API5 and AIP1/2, we compared the expression profiles between the wild type and *api5* using Affymetrix rice chips with RNAs from anthers at late stages 8/9. In the preliminary data, a rice Cys protease gene *CP1* was down-regulated 2-fold in *api5*. *CP1* was identified as the direct target of *TDR*, which is established to be involved in tapetal PCD in rice (Li et al., 2006). Suppressed expression of *CP1* caused a significant defect in pollen development (Lee et al., 2004), with similar phenotypes to those of *api5* and *amiRNA-AIP1/2* transgenic plants. qRT-PCR analysis verified that the transcript level of *CP1* in anthers decreased dramatically in the *api5* mutants (Figure 11A). Interestingly, greatly reduced expression of *CP1* was also detected in the *amiR-AIP1/2* transgenic plants (S81 and S82; Figure 11B). This result suggested that *CP1* was positively regulated by API5 and AIP1/2.

To examine whether API5 and AIP1 regulate *CP1* directly, we used yeast one-hybrid assays to test the potential interactions between API5/AIP1 and the promoter of *CP1*. The region of the *CP1* promoter was divided into two ~100-bp overlapping fragments (CP1-P-1 and CP1-P-2) for the one-hybrid assays in yeast. Results showed that AIP1 interacted with CP1-P-1 (−377 to −272, relative to the start codon) in yeast (Figures 11C and 11D), but failed to bind to CP1-P-2 (−170 to −59, relative to the start codon). However, no interaction between API5 and the promoter of *CP1* was observed. EMSA competition experiments were conducted to assess the binding ability of AIP1 with CP1-P-1 in vitro. As shown in Figure 11E, Os AIP1 binding activity was greatly reduced in the presence of unlabeled CP1-P-1 fragments as competitors. Furthermore, a chromatin immunoprecipitation (ChIP) assay showed that the anti-AIP1 antibody specifically precipitated with promoter region CP1-P-1 of *CP1* (Figure 11F). These results strongly indicate that AIP1 regulates the degeneration of tapetum through its direct target gene *CP1*.

Li et al. (2006) reported that TDR could bind directly to a 160-bp promoter region (−673 to −513, relative to the start codon) of *CP1*. This common target of AIP1 and TDR prompted us to speculate that API5, AIP1/2, and TDR may exist in a transcriptional complex. However, yeast two-hybrid results showed that TDR exhibited no direct interaction with API5, AIP1, or AIP2 (see Supplemental Figure 7 online). It indicated that TDR and API5-Os AIP1/2 may perform tapetal PCD functions in distinct transcriptional complexes.

Based on the common target of TDR and API5-AIP1/2 in regulation of tapetal PCD in rice, we compared the gene expression network in individual mutant backgrounds. As expected, the expression of *CP1* was down-regulated in *tdr* compared with the wild type (see Supplemental Figure 8A online). Interestingly, the expression of *API5* was upregulated in *tdr*, and no obvious difference in the expression level of *AIP1/2* was detected between *tdr* and the wild type (see Supplemental Figures 8B and 8C online). This indicated that a feedback regulation may exist to promote the expression of *API5* in case of loss of function of *TDR*. Next, we further compared the expression pattern of downstream genes of *TDR* in *api5*. Some down-regulated genes in *tdr*, *Os03g07140* and *Os03g21380*, involved in synthesis of fatty alcohols and encoding a putative calcium-binding protein, respectively (Zhang et al., 2008), were dramatically suppressed in *api5* (see Supplemental Figures 8D to 8J online). By contrast, the expression of other genes (*C6* and *RAFTIN1*) involved in lipid transfer and pollen exine formation (Wang et al., 2003; Zhang et al., 2010) were not affected in *api5* (see Supplemental Figures 8E and 8G online). These data suggest that API5 and TDR may have other common functions in the synthesis of fatty alcohols, in addition to regulating tapetal PCD.

DISCUSSION

API5 Is a Positive Regulator of Tapetal PCD in Rice

Based on genetic and cytologic analyses of the *api5* mutant, we demonstrated that API5 is a critical positive regulator of the PCD process in tapetum degradation in rice. Although the expression of *API5* is widely detected, its enhanced expression in tapetum is consistent with its function in the tapetum PCD process. Previous reports showed that premature or delayed tapetal PCD results in defects in pollen formation (Ku et al., 2003; Li et al., 2006). Our data revealed that the partially inhibited PCD process in *api5* led to pollen sterility, suggesting that the extent of PCD in the tapetum is important for pollen development.

At the molecular level, API5 regulates the expression of the target gene via its partner, AIP1/2, which binds the promoter of *CP1*. Suppressed expression of *CP1* resulted in similar mutant phenotypes as those seen in *api5* (Lee et al., 2004). Cys proteases represent a family of enzymes with important roles in intracellular protein degradation and are associated with PCD in animals, plants, and microorganisms (Solomon et al., 1999). More importantly, as reported by Li et al. (2006), a bHLH transcription factor, TDR, can also bind directly to the promoter of *CP1*, whereas mutation of *TDR* resulted in retardation of tapetum degradation caused by inhibited PCD of the tapetum and defects in pollen development (Zhang et al., 2008). Taken together, we propose that the expression of *CP1* or regulators that control the expression of *CP1*, such as TDR, API5, and AIP1/2, are critical for the degeneration of the tapetum. Although AIP1 and TDR bind different sites on the promoter of *CP1*, no interaction between them was observed, suggesting that other factors may or may not also be mediating the interaction between them.

In addition to the delayed tapetum degradation observed in both *api5* and *tdr*, exine formation in the pollen was also defective in the *tdr* mutant (Zhang et al., 2008), whereas the exine of pollen in *api5* was normal (see Supplemental Figure 2 online). Moreover, three down-regulated genes in *tdr* (*C6*, *C4*, and *RAFTIN1*), which were characterized as being involved in pollen wall formation (Wang et al., 2003; Zhang et al., 2008, 2010), showed no obvious expression difference in *api5*. These results suggest that *TDR* and *API5* might regulate a cluster of genes among different

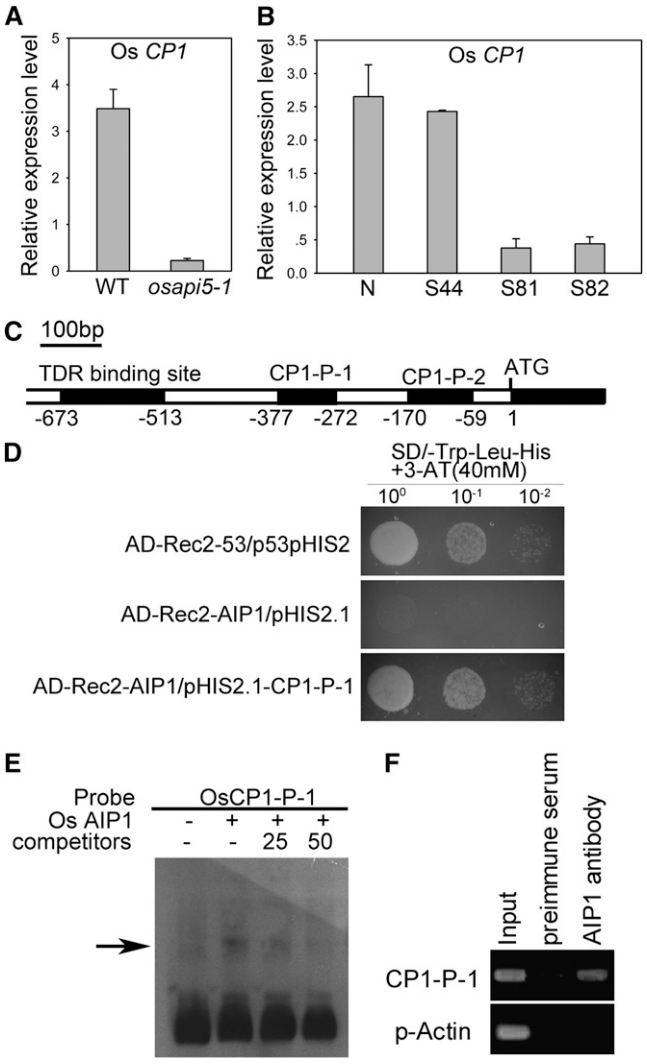

Figure 11. Binding Assays of AIP1 with the Promoter Region of *CP1*.

(A) The transcript levels of *CP1* in spikelets of the wild type (WT) and *api5* at stage 8/stage 9. The data shown are the means ± SEM of three biologic replicates. Rice *Ubiquitin5* was used as the internal control.

(B) The transcript levels of *CP1* in *amiR-AIP1/2* transgenic plants. The data shown are the means ± SEM of three RNA extraction experiments. Rice *Ubiquitin5* was used as the internal control.

(C) Schematic diagram of binding regions of TDR and AIP1 in the promoter of *CP1*. The leftmost black boxes represent binding regions of TDR. The other two black boxes labeled with CP1-P-1 and CP1-P-2 mark the regions used for detecting their interaction with AIP1 in yeast one-hybrid assays. The numbers indicate the position relative to the start codon.

(D) Binding of Os AIP1 to a 106-bp promoter region of Os *CP1* in yeast one-hybrid assays; a well-known interaction of p53 and its binding region (pGAD-Rec2-53/p53pHIS2) was used as a positive control, with expression of Os AIP1 alone and empty pHIS2.1 vector used as negative control.

(E) Gel shift assays of AIP1 interacting with a promoter region (CP1-P-1) of *CP1* with a length of 106 bp. *E. coli*-produced recombinant Os AIP1 protein was incubated with digoxin-labeled CP1-P-1 in the absence or presence of 25- or 50-fold molar excess of the unlabeled probes as competitor for the electrophoretic mobility shift assay (EMSA) reaction and analyzed by electrophoresis. The shifted band is indicated by an arrow.

(F) ChIP assays using the wild-type spikelets at stages 8/9 showed that AIP1 binds to the promoter of *CP1 in vivo*. Immunoprecipitation was performed with anti-Os AIP1 antibody and preimmune serum. Input lane represents PCR products with templates of purified DNA from isolated chromatin; Preimmune serum lane represents PCR products with templates of purified DNA from immunoprecipitated chromatin by preimmune serum (no antibody); AIP1 antibody lane represents PCR products with templates of purified DNA from immunoprecipitated chromatin by AIP1 antibody. An unrelated DNA fragment from the rice *Actin1* gene was used as a control.

pathways, with their overlapping function restricted to influencing the degeneration of tapetum by regulation *CP1*.

Os API5 is a member of the Api5 family, which is an ancient and conserved protein superfamily present in protists, plants, and animals (Figure 6). Studies in mammals have demonstrated that AAC-11/API5 is an antiapoptotic factor (Tewari et al., 1997). A recent investigation showed that Api5 suppresses specifically E2F1-induced apoptosis without altering E2F-dependent transcription in *Drosophila*; this genetic interaction between Api5 and E2F1 is conserved in humans (Morris et al., 2006). As shown in another report, AAC-11 can physiologically bind to Acinus and prevent Acinus-mediated DNA fragmentation, implying that AAC-11 has an antiapoptotic effect on drug-induced cell death (Rigou et al., 2009). However, our results suggested Os API5 to be a positive regulator of PCD. Nonetheless, these results indicate that there may exist an essential and conserved function of API5 in PCD or apoptosis regulation among eukaryotes, although the details may differ.

Roles of AIP1 and AIP2 in Regulating PCD of the Tapetum

AIP1 and AIP2 are nearly identical proteins; they differ in only three amino acids that do not influence their interactions with API5. Analyses of *amiRNA-AIP1/2*-mediated transgenic plants indicated that AIP1 and AIP2 are also essential positive regulators for tapetum degeneration. In plants, several DEAD-box RNA helicases have been identified that are involved in development and stress responses. The *Arabidopsis* LOS4, CRYOPHYTE, PMH1/PMH2, SRS1/SRS2, and rice BIRH1 are involved in responses to biotic and abiotic stresses (Gong et al., 2002, 2005; Kant et al., 2007; Matthes et al., 2007; Li et al., 2008), whereas other DEAD-box RNA helicases are involved in development. For example, tobacco VDL and CAF are required for suppression of cell division in floral meristems and plant morphogenesis, respectively (Jacobsen et al., 1999; Wang et al., 2000). Both Os *AIP1* and Os *AIP2* encode DEAD-box ATP-dependent RNA helicases. Similar to Os API5, Os AIP1 and AIP2 are also highly conserved proteins that exist widely in different species. The homologs of Os AIP1/2 in animals are involved in nearly all aspects of mRNA metabolism, including transcription, splicing, export of mRNA, and translation (de la Cruz et al., 1999; Rocak and Linder, 2004). The homolog of Os AIP1 and Os AIP2 in yeast is SUB2p, which is the functional homolog of hUAP56. It is well

known that SUB2p and hUAP56 are components of the conserved TREX complex and mediate the coupling of transcription elongation and export of nuclear mRNA (Strässer et al., 2002). Another report showed that hUAP56 is a component of a protein complex that binds directly to a conserved fragment of the cytochrome *c* gene promoter (Goffart et al., 2006). Our results demonstrated that Os AIP1/2 could bind the specific promoter region of Os *CP1*. Therefore, the role of Os AIP1/2 in mediating the interaction between Os API5 and its target genes seems to be as a "bridge" protein. However, in addition to the different subcellular localizations between monomeric Os AIP1/2 and dimeric Os AIP1/2, an overlapping subcellular localization between dimeric Os AIP1/2 and Os API5 was found. It is possible that Os AIP1/2 is involved in biological functions in the cytoplasm other than in transcription regulation.

PCD in the Rice Tapetum Is Governed by the API5-AIP1/2-*CP1* Pathway

Here we report Os API5, a putative ortholog of AAC-11 in humans, acts as a positive regulator in PCD. Our molecular genetic studies of Os *API5* led to the identification of an API5-AIP1/2 complex. This complex acts on *CP1* by binding directly to its promoter region, thus regulating its expression. Supported by the previous research in TDR (Li et al., 2006), we propose a pathway that regulates PCD during tapetum degeneration in rice. At the meiosis stage of pollen development, the tapetal cells receive the signals and are ready to provide nutrient and signal molecules for pollen development by PCD. TDR is expressed and then binds to the promoter region of *CP1*. Finally, the designated transcription initiation complex enhances the expression of *CP1*, an executor of the PCD process, resulting in the initiation of tapetum degeneration at the tetrad stage. Loss of function of *API5* or down-regulation of *AIP1/2* results in a failure to form the transcription initiation machineries, and the expression of *CP1* is suppressed even in the presence of TDR, and thus degeneration of the tapetum is inhibited. This model provides insight into the roles of API5, AIP1/2, and CP1 in regulating tapetum PCD. We also noticed that API5, AIP1/2, CP1, and even TDR, are all highly conserved in their own protein families and widely distributed in different species. It is known that the expression of API5 is usually upregulated in tumor cells, especially in metastatic cells. As the depletion of API5 resulted in tumor cell death, API5 was selected as a candidate for antitumor therapy target (Faye and Poyet, 2010). However, in our study, Os API5 was examined as a positive regulator for the PCD process during tapetal degeneration in rice. How API5 in humans and rice obtained opposite roles in PCD processes during evolution is still an open question.

METHODS

Isolation of T-DNA Insertion Mutants

The mutant line 03Z11RO53 (*api5-1*; rice [*Oryza sativa* ssp *japonica* cv Zhonghua 11]) was obtained from the RMD database (Wu et al., 2003; Zhang et al., 2006a; http://rmd.ncpgr.cn/) and 3A-10121 (*api5-2*; rice ssp *japonica* cv Dongjin) was ordered from the POSTECH RISD database (Jeon et al., 2000; http://www.postech.ac.kr/life/pfg/risd/), respectively. Mutants were planted in the paddy field of Huazhong Agricultural University in the normal rice (*Oryza sativa*) growing season of Wuhan, China, and in a greenhouse during the winter. All transgenic plants were grown in similar growth conditions.

Constructs and Rice Transformation

For the functional complementation test, the 15.1-kb genomic DNA fragment containing the entire Os *API5* coding region and the 1.6-kb upstream and 4.4-kb downstream sequence was obtained by *Bam*HI digestion of the Clemson BAC clone OSJNBa0019G21 (kindly provided by R. Wing, University of Arizona) and inserted into the binary vector pCAMBIA2301 (http://www.cambia.org). An empty pCAMBIA2301 vector was used as a negative control. Homozygous callus from *api5* as transformation recipient was selected by genotyping of callus culture induced from seeds harvested from *API5/api5* heterozygous plants.

For overexpression of artificial micro-RNA of the Os *AIP1/2* construct, the 250-bp fragment containing 21mers recognizing specifically the 3′ untranslated region of Os *AIP1* and Os *AIP2* transcripts simultaneously was amplified using universal primers G11491/G11494 and specific primers, including AIP-miR-I, II, III, and IV, which were designed in WMD2 (http://wmd2.weigelworld.org) as described previously (Warthmann et al., 2008), and then cloned into *Kpn*I-*Bam*HI-digested pU1301 (Chu et al., 2006). For overexpression of *API5*, full-length cDNA was amplified with primer pair Api5 OX-F/Api5 OX-R and then cloned into pU1301 by *Kpn*I-*Bam*HI digestion. All the constructs were introduced into *Agrobacterium tumefaciens* EHA105 and were transformed into the callus derived from japonica cultivar Zhonghua 11 by *Agrobacterium*-mediated transformation as previously described (Wu et al., 2003). All primers for genotyping and vector construction are listed in Supplemental Table 1 online.

Histochemical Assays and Microscopic Analyses

To evaluate the viability of mature pollen grains, anthers from mature flowers were dissected in a drop of iodium potassium iodide solution, and images were captured with a DFC480 Digital Camera system (Leica; Chang et al., 2009). For cytohistological analyses, spikelets of various anther developmental stages and vegetative tissues were fixed in a solution containing 50% ethanol (70% ethanol for fixation of vegetative tissues), 5% glacial acetic acids, and 3.7% formaldehyde for 24 h at room temperature and were then replaced with 70% ethanol twice. Fixed anthers were dehydrated through an ethanol series, embedded into Technovit 7100 resin (Heraeus Kulzer), and polymerized at 37°C for 3 d. The sample blocks were sectioned into 2-μm thick slices with a microtome (Leica) and stained with 0.25% toluidine blue O (Merck). Images were captured with a DFC480 Digital Camera system (Leica).

For TEM, anthers at various developmental stages were prefixed with 2.5% glutaraldehyde in 0.1 M sodium phosphate buffer (pH 7.4), and were then fixed in 2% OsO_4 in phosphate-buffered saline (pH 7.4). Following ethanol dehydration, samples were embedded in epoxy resin (London Resin Company). Ultrathin sections (70 nm) were obtained using a UC6 ultramicrotome (Leica) and were then double stained with 2% (w/v) uranyl acetate and 2.6% (w/v) lead citrate aqueous solution. Observation and capturing of images were performed with a H-7650 transmission electron microscope (Hitachi) at 80 kV and an 832 charge-coupled device camera (Gatan).

TUNEL Assays

Anthers at different developmental stages were fixed in a solution containing 50% ethanol, 5% glacial acetic acids, and 3.7% formaldehyde for 24 h at 4°C. Eight micrometer paraffin sections of treated anthers were

used for in situ nick-end labeling of nuclear DNA fragmentation with a TUNEL apoptosis detection kit (DeadEnd Fluorometric TUNEL system; Promega) according to the supplier's instructions. The green fluorescence of fluorescein and red fluorescence of propidium iodide were analyzed at 520 ± 10 nm and 640 ± 10 nm, respectively, under a laser-scanning confocal microscope (TCS SP2; Leica).

Comet Assay for DNA Damage

Anthers of different developmental stages were chopped with a razor in a Petri dish with a diameter of 5 cm containing 500 mL of ice-cold PBS plus 20 mM EDTA. The comet assay kit (Trevigen) was used for single cell gel electrophoresis assays according to the supplier's manuals, and images were captured with a DFC480 digital camera system (Leica). The percentage of DNA in each comet tail (T DNA%) was evaluated with CometScore software (http://www.autocomet.com). The extent of DNA damage in each nucleus is designated by the units 0, 1, 2, or 3. An increased unit correlated with a higher DNA percentage in the tail, as shown in the demonstration in Figure 3. This categorization was described by Wang and Liu (2006).

RT-PCR and qRT-PCR

Total RNA was isolated from roots, stem, leaf sheath, leaves, and young panicles of rice using TRIzol reagent (Invitrogen). Total RNA (3 μg) was reverse transcribed by M-MLV RT (Promega) with the oligo (dT) 20 primer, and 1 μL of RT product was used as template for RT-PCR. qPCR was performed in an optical 96-well plate that included *SYBR Premix EX Taq* and 0.5 μL of Rox Reference Dye II (Takara), 1 μL of the cDNA sample, and 0.2 μM of each gene-specific primer, in a final volume of 25 μL on a PRISM 7500 PCR instrument (Applied Biosystems). The reactions were performed at 95°C for 10 s, 45 cycles of 95°C for 5 s, and 60°C for 40 s. Disassociation curve analysis was performed as follows: 95°C for 15 s, 60°C for 20 s, and 95°C for 15 s. Data were collected using the ABI PRISM 7500 sequence detection system following the instruction manual. The rice *Ubiquitin5* gene was used as the internal control. The amiR-AIP-St-RT primer and amiR-AIP-forward primer were used for detecting the mature *amiR-AIP1/2* levels by qRT-PCR as previously described (Chen et al., 2005). U6 was used as an internal control. All primers for RT-PCR and qRT-PCR are listed in Supplemental Table 2 online.

In Situ Hybridization

Spikelets from different developmental stages were fixed in a solution containing 50% ethanol, 5% acetic glacial, and 3.7% formaldehyde for 16 h at 4°C, and were then replaced with 70% ethanol twice and dehydrated with ethanol series, substituted with xylene, embedded in paraffin, and sectioned to 8 μm. Os *API5* and *AIP1* cDNA fragments were amplified with the primer pairs API5FL-F/ R and AIP-in-F/R and then ligated into the pGEM-T vector (Promega). The probe was then transcribed in vitro from the T7 or SP6 promoter with polymerase using a digoxigenin RNA labeling kit (Roche). RNA hybridization and immunologic detection of the hybridized probes were performed according to the protocol of (DeBlock and Debrouwer, 1993).

Subcellular Localization of Os API5 and Os AIP1/2

To construct the subcellular localization plasmids, the full-length CDSs of API5, AIP1, and AIP2 were amplified with specific template by primers API5-M99-F, API5-M99-R, AIP-M99-F, and AIP-M99-R with *Xba*I digestion sites and were inserted into pM999-YFP (kindly provided by Jian Xu, National University of Singapore) for fusion with the reporter gene. Mesophyll protoplasts were isolated from 5-week-old *Arabidopsis thaliana* (ecotype Columbia) and transformed with the tested pairs (pM999-CFP-GHD7 was kindly provided by Lei Wang, Huazhong Agricultural University) of constructs (http://genetics.mgh.harvard.edu/sheenweb/protocols_reg.html). Fluorescence in the transformed protoplasts was imaged using a confocal laser scanning microscope (TCS SP2; Leica) after incubation at 23°C for 12 to18 h.

Transactivation Activity Assay

To construct a series of GAL4 BD-fused full-length or truncated Os API5 constructs to test for transcriptional activity, the CDS of Os API5 was amplified with primers API5-BK-F, API5(N104)-BK-F, API5(N116)-BK-F, and API5(N243)-BK-F (see Supplemental Table 1 online) paired to API5-BK-R with an adapter containing *Eco*RI-*Bam*HI digestion sites, and then cloned into pGBK-T7 (http://www.clontech.com/) to add the GAL4 BD. The assays for transactivation activity were performed in yeast (*Saccharomyces cerevisiae*) strain AH109. All vectors, including full-length or truncated Os API5, fused the GAL4 BD and were transformed into yeast strain AH109. Transformants were plated on either tryptophan-negative synthetic dropout medium (SD/–Trp) or tryptophan-negative and adenine-negative synthetic dropout medium (SD/–Trp–Ade).

Yeast Two-Hybrid Assay

To test the interaction between TDR and Os API5 or Os AIP1/2, full-length CDSs of Os *AIP1* and Os *AIP2* were amplified by primer pairs AIP-BK-F/AIP-BK-R with adapters (see Supplemental Table 1 online) for *Nde*I-*Eco*RI digestion sites and cloned into pGBK-T7 and pGAD-T7 (Clontech), respectively. To generate pGAD-TDR, the *Eco*RI-*Bam*HI–digested fragment from pGBK-TDR (kindly provided by D.B. Zhang, Shanghai Jiao Tong University), which contained the CDS of TDR, was cloned into *Eco*RI-*Bam*HI–digested pGAD-T7 for characterizing the interaction with Os API5 or Os AIP1/2. Total RNA for construction of the yeast AD-fused cDNA library was prepared from rice panicles with a length of 3 cm using Matchmaker Library Construction and Screening Kits (Clontech). The library was screened using full-length Os API5 as bait by yeast mating. The Matchmaker GAL4 Two-Hybrid System 3 was used for confirmation of the dimerization of Os AIP1/2 and the interaction between TDR and Os API5 or Os AIP1/2.

BiFC Assays

BiFC assays were performed as described previously (Walter et al., 2004). For generation of the BiFC vectors, the CDS of Os *API5* was amplified with primer pairs AIP-BiFC-F/AIP-BiFC-R (see Supplemental Table 1 online) and cloned at *Spe*I-*Kpn*I sites in pUC-SPYNE (http://www.uni-muenster.de/Biologie.Botanik/agkudla/Plasmids.html) and the CDS of Os *AIP1* was cloned into *Spe*I-*Kpn*I sites of pUC-SPYNE and pUC-SPYCE, resulting in pUC-SPYNE-API5, pUC-SPYNE-AIP1, and pUC-SPYCE-AIP1. *Arabidopsis* mesophyll protoplasts were prepared and transformed with different combinations of constructs and imaged for fluorescence of YFP as mentioned in the section "Subcellular Localization of Os API5 and OS AIP1/2."

Co-IP

Co-IP assays were performed using the Matchmaker Co-IP kit (Clontech). ^{35}S-labeled c-*myc*-fused Os API5 and HA-fused Os AIP1 were translated in vitro using the plasmids of pGBK-API5 and pGAD-AIP1 as templates, respectively, by the TNT T7 Coupled Reticulocyte Lysate System (Promega). The Co-IP reaction was performed according to the manufacturer's instructions. In brief, the anti-myc antibody and c-*myc*-fused Os API5 mix was added to a tube containing protein A beads, meanwhile, the anti-HA antibody and HA-fused Os AIP1 mix was added to another tube containing protein A beads. After gentle mixing, HA-fused Os AIP1 and c-*myc*-fused Os API5 was added into the tube, respectively.

Following gentle mixing again and a washing step, the reaction products were loaded onto 12% SDS-PAGE gels, and then the signals were obtained by autoradiography of the dried gel.

Multiple Sequence Alignment and Construction of the Phylogenetic Tree

The multiple sequence alignment was performed by ClustalW (http://www.ebi.ac.uk/clustalw/) with parameters of Weight matrix: Gonnet; Gap opening penalty: 10.0 and Gap extension penalty: 0.20. A phylogenetic tree was constructed with the aligned API5 protein sequences (see Supplemental Data Set 1 online) using MEGA 3.1 software (http://www.megasoftware.net/index.html; Kumar et al., 2004) based on the neighbor-joining method with parameters of Poisson correction model, pairwise deletion, and bootstrap (1000 replicates; random seed).

Complementation Test of Yeast *sub2* Mutant

The heterozygous diploid yeast strain BY4743 (*sub2*::*G418*/*SUB2*) was obtained from Invitrogen (cat. No. 95400, clone ID: 23,781). The strain was transformed with pGAD-AIP1 and pGAD-AIP2, individually. The transformants were induced for sporulation in liquid sporulation medium according to the method described at the website: http://www-sequence.stanford.edu/group/yeast_deletion_project/spo.html. The cultures were checked on SD/−Leu, SD/−Met/G418, and SD/−Lys/G418, respectively.

Yeast One-Hybrid Assay

To characterize the interaction between Os AIP1 and the promoter region of Os *CP1* in yeast, the *Eco*RI-*Sac*I–digested fragment containing full-length cDNA from pGAD-Rec-AIP1, a positive clone isolated from yeast two-hybrid library screening, was cloned into *Eco*RI-*Sac*I–digested pGAD-Rec2 (Clontech), thus generating pGAD-Rec2-AIP1 for yeast one-hybrid. The promoter region of Os *CP1* was amplified by primer pair CP1-P1-F/CP1-P1-R (see Supplemental Table 1 online) with adapters containing *Eco*RI-*Sac*I digestion sites and cloned into pHIS2.1 (Clontech). Yeast strain Y187 was transformed with pGAD-Rec2-AIP1 and pHIS2.1-CP1-P1 and positive clones were selected on synthetic dropout medium.

EMSA

To express the Os AIP1 in *Escherichia coli*, the CDS of Os *AIP1* was amplified with primers AIP28a-F and AIP28a-R cloned into the *Eco*RI-*Hin*dIII sites of the pET-28a (Novagen) and introduced into BL21 (DE3) cells (Novagen). The transformed cells were cultured at 37°C until the OD600 of the cell culture was 0.5, and then was induced with 1mM isopropyl-1-thio-b-D-galactopyranoside for 4 h at 30°C. His-tagged Os AIP1 was extracted and purified with Ni-NTA agarose (Qiagen). The promoter region of Os *CP1* was amplified with primers CP1-P1-F and CP1-P1-R to use as a probe. Probe labeling, binding reactions, and detection of probe shifts were performed using the DIG Gel Shift Kit (2nd Generation; Roche) according to the manufacturer's instructions.

ChIP Assays

The specific AIP1 antibody was made and purified by Neweast Biotechnology. Briefly, 5 mg of purified His-AIP1 protein was used to immunize rabbits at 3-week intervals. AIP1-specific antibodies were purified from the crude rabbit antiserum on a column in which the same His-AIP1 had been covalently attached to cyanogen bromide-activated Sepharose. The specificity of the Os AIP1 antibody was tested by a competition experiment in which the antibody was mixed with an excessive amount of the His-AIP1 protein. The mixture and the Os AIP1 antibody were used as the probe to hybridize with membrane blotted with *E. coli*-expressed Os AIP1 proteins and nucleic extract from the spikelet at stages 8/9, respectively. The results showed that Os AIP1 antibody was specific (see Supplemental Figure 9 online).

Immunoprecipitations were performed as described previously (Bowler et al., 2004). In brief, the wild-type rice anthers at stages 8/9 were fixed in formaldehyde in a vacuum. The chromatin solution was sonicated and the soluble chromatin fragments were obtained from isolated nuclei. Preadsorption with sheared salmon sperm DNA/Dynabeads protein A (Invitrogen) was performed to remove nonspecific binding DNA. Immunoprecipitation with AIP1-specific antibody and preimmune serum was performed as described. Immunoprecipitated DNA was analyzed by PCR using primers CP1-P1-F/CP1-P1-R and p-Actin-F/p-Actin-R (see Supplemental Table 1 online) with 30 cycles of PCR, and the products were analyzed by agarose gel electrophoresis.

Accession Numbers

Sequence data from this article can be found in the GenBank/EMBL databases under the following accession numbers: Os *API5* (Os02g0313400), Os *AIP1* (Os01g0549700), Os *AIP2* (Os01g0550000), *TDR* (Os02g0120500), Os *CP1* (Os04g0670500), Os *C6* (Os11g0582500), Os *C4* (Os08g0546300), Os *RAFTIN1* (Os08g0496800), hUAP56 (Q13838), and SUB2p (CAA98650). The accession numbers for the proteins used in the phylogenetic analysis are given in the labels on Figure 6.

Supplemental Data

The following materials are available in the online version of this article.

Supplemental Figure 1. Comparison of Transverse Sections during Early Anther Development from the Wild Type and *api5-1*.

Supplemental Figure 2. Pollen Wall Development in the Wild Type and *api5-1*.

Supplemental Figure 3. Genotyping and Complementation of *api5-1*.

Supplemental Figure 4. Characterization of Phenotypes of *api5-2*.

Supplemental Figure 5. Characterization of Os *API5*-Overexpressing Plants and Histologic Comparison of Vegetative Tissues among *api5-1*, the Wild Type, and Os *API5*-Overexpressing Plants.

Supplemental Figure 6. Expression Analysis of *AIP1/2* in *api5-1* and the Wild Type.

Supplemental Figure 7. Interaction Tests of TDR with Os API5, Os AIP1, and Os AIP2 by Yeast Two-Hybrid Assay.

Supplemental Figure 8. qRT-PCR Analyses of Rice Genes Related to Anther Development in *tdr* and *api5*.

Supplemental Figure 9. Analysis of the Specificity of AIP1 Polyclonal Antibodies.

Supplemental Table 1. Primers for Genotyping and Plasmid Construction.

Supplemental Table 2. Primers for RT-PCR, qRT-PCR, and ChIP-PCR.

Supplemental Data Set 1. Text File of the Protein Sequence Alignment of Os API5 with Other Members of the API5 Family Used to Generate the Phylogenetic Tree.

ACKNOWLEDGMENTS

We thank Dabing Zhang for providing the plasmid pGBK-TDR and transcripts of *tdr*, Jian Xu for providing the plasmid pM999, and G. An for

providing the T-DNA insertional line 3A-10121. We thank Jialing Yao and Jianbo Cao for technical assistance. We also thank Dabing Zhang for assistance in revising the manuscript. This research was supported by grants from the National Program on Key Basic Research Project, National Special Key Project of China on Functional Genomics of Major Plants and Animals, and the National Natural Science Foundation of China.

Received December 21, 2010; revised February 15, 2011; accepted February 28, 2011; published April 5, 2011.

REFERENCES

Aya, K., Ueguchi-Tanaka, M., Kondo, M., Hamada, K., Yano, K., Nishimura, M., and Matsuoka, M. (2009). Gibberellin modulates anther development in rice via the transcriptional regulation of GAMYB. Plant Cell **21:** 1453–1472.

Bowler, C., Benvenuto, G., Laflamme, P., Molino, D., Probst, A.V., Tariq, M., and Paszkowski, J. (2004). Chromatin techniques for plant cells. Plant J. **39:** 776–789.

Chang, Y., Gong, L., Yuan, W., Li, X., Chen, G., Li, X., Zhang, Q., and Wu, C. (2009). Replication protein A (RPA1a) is required for meiotic and somatic DNA repair but is dispensable for DNA replication and homologous recombination in rice. Plant Physiol. **151:** 2162–2173.

Chen, C., et al. (2005). Real-time quantification of microRNAs by stem-loop RT-PCR. Nucleic Acids Res. **33:** e179.

Chen, R., Zhao, X., Shao, Z., Wei, Z., Wang, Y., Zhu, L., Zhao, J., Sun, M., He, R., and He, G. (2007). Rice UDP-glucose pyrophosphorylase1 is essential for pollen callose deposition and its cosuppression results in a new type of thermosensitive genic male sterility. Plant Cell **19:** 847–861.

Chu, Z., Yuan, M., Yao, J., Ge, X., Yuan, B., Xu, C., Li, X., Fu, B., Li, Z., Bennetzen, J.L., Zhang, Q., and Wang, S. (2006). Promoter mutations of an essential gene for pollen development result in disease resistance in rice. Genes Dev. **20:** 1250–1255.

de la Cruz, J., Kressler, D., and Linder, P. (1999). Unwinding RNA in *Saccharomyces cerevisiae*: DEAD-box proteins and related families. Trends Biochem. Sci. **24:** 192–198.

De Block, M., and Debrouwer, D. (1993). RNA-RNA in situ hybridization using digoxigenin-labeled probes: The use of high-molecular-weight polyvinyl alcohol in the alkaline phosphatase indoxyl-nitroblue tetrazolium reaction. Anal. Biochem. **215:** 86–89.

Faye, A., and Poyet, J.L. (2010). Targeting AAC-11 in cancer therapy. Expert Opin. Ther. Targets **14:** 57–65.

Goffart, S., Franko, A., Clemen, C.S., and Wiesner, R.J. (2006). α-Actinin 4 and BAT1 interaction with the cytochrome c promoter upon skeletal muscle differentiation. Curr. Genet. **49:** 125–135.

Goldberg, R.B., Beals, T.P., and Sanders, P.M. (1993). Anther development: Basic principles and practical applications. Plant Cell **5:** 1217–1229.

Gong, Z., Dong, C.H., Lee, H., Zhu, J., Xiong, L., Gong, D., Stevenson, B., and Zhu, J.K. (2005). A DEAD box RNA helicase is essential for mRNA export and important for development and stress responses in *Arabidopsis*. Plant Cell **17:** 256–267.

Gong, Z., Lee, H., Xiong, L., Jagendorf, A., Stevenson, B., and Zhu, J.K. (2002). RNA helicase-like protein as an early regulator of transcription factors for plant chilling and freezing tolerance. Proc. Natl. Acad. Sci. USA **99:** 11507–11512.

Ito, T., Nagata, N., Yoshiba, Y., Ohme-Takagi, M., Ma, H., and Shinozaki, K. (2007). *Arabidopsis* MALE STERILITY1 encodes a PHD-type transcription factor and regulates pollen and tapetum development. Plant Cell **19:** 3549–3562.

Jacobsen, S.E., Running, M.P., and Meyerowitz, E.M. (1999). Disruption of an RNA helicase/RNAse III gene in Arabidopsis causes unregulated cell division in floral meristems. Development **126:** 5231–5243.

Jeon, J.S., et al. (2000). T-DNA insertional mutagenesis for functional genomics in rice. Plant J. **22:** 561–570.

Jung, K.H., Han, M.J., Lee, Y.S., Kim, Y.W., Hwang, I., Kim, M.J., Kim, Y.K., Nahm, B.H., and An, G. (2005). Rice Undeveloped Tapetum1 is a major regulator of early tapetum development. Plant Cell **17:** 2705–2722.

Kant, P., Kant, S., Gordon, M., Shaked, R., and Barak, S. (2007). STRESS RESPONSE SUPPRESSOR1 and STRESS RESPONSE SUPPRESSOR2, two DEAD-box RNA helicases that attenuate Arabidopsis responses to multiple abiotic stresses. Plant Physiol. **145:** 814–830.

Kawanabe, T., Ariizumi, T., Kawai-Yamada, M., Uchimiya, H., and Toriyama, K. (2006). Abolition of the tapetum suicide program ruins microsporogenesis. Plant Cell Physiol. **47:** 784–787.

Ku, S., Yoon, H., Suh, H.S., and Chung, Y.Y. (2003). Male sterility of thermosensitive genic male-sterile rice is associated with premature programmed cell death of the tapetum. Planta **217:** 559–565.

Kumar, S., Tamura, K., and Nei, M. (2004). MEGA3: Integrated software for Molecular Evolutionary Genetics Analysis and sequence alignment. Brief. Bioinform. **5:** 150–163.

Lee, S., Jung, K.H., An, G., and Chung, Y.Y. (2004). Isolation and characterization of a rice cysteine protease gene, *OsCP1*, using T-DNA gene-trap system. Plant Mol. Biol. **54:** 755–765.

Li, D., Liu, H., Zhang, H., Wang, X., and Song, F. (2008). OsBIRH1, a DEAD-box RNA helicase with functions in modulating defense responses against pathogen infection and oxidative stress. J. Exp. Bot. **59:** 2133–2146.

Li, N., et al. (2006). The rice *tapetum degeneration retardation* gene is required for tapetum degradation and anther development. Plant Cell **18:** 2999–3014.

Ma, H. (2005). Molecular genetic analyses of microsporogenesis and microgametogenesis in flowering plants. Annu. Rev. Plants Biol. **56:** 393–434.

Matthes, A., Schmidt-Gattung, S., Köhler, D., Forner, J., Wildum, S., Raabe, M., Urlaub, H., and Binder, S. (2007). Two DEAD-box proteins may be part of RNA-dependent high-molecular-mass protein complexes in Arabidopsis mitochondria. Plant Physiol. **145:** 1637–1646.

McCormick, S. (1993). Male gametophyte development. Plant Cell **5:** 1265–1275.

Morris, E.J., Michaud, W.A., Ji, J.Y., Moon, N.S., Rocco, J.W., and Dyson, N.J. (2006). Functional identification of Api5 as a suppressor of E2F-dependent apoptosis in vivo. PLoS Genet. **2:** e196.

Pacini, E., Franchi, G., and Hesse, M. (1985). The tapetum: Its form, function, and possible phylogeny in *Embryophyta*. Plant Syst. Evol. **149:** 155–185.

Papini, A., Mosti, S., and Brighigna, L. (1999). Programmed-cell-death events during tapetum development of angiosperms. Protoplasma **207:** 213–221.

Rigou, P., Piddubnyak, V., Faye, A., Rain, J.C., Michel, L., Calvo, F., and Poyet, J.L. (2009). The antiapoptotic protein AAC-11 interacts with and regulates Acinus-mediated DNA fragmentation. EMBO J. **28:** 1576–1588.

Rocak, S., and Linder, P. (2004). DEAD-box proteins: The driving forces behind RNA metabolism. Nat. Rev. Mol. Cell Biol. **5:** 232–241.

Scott, R., Hodge, R., Paul, W., and Draper, J. (1991). The molecular biology of anther differentiation. Plant Sci. **80:** 167–191.

Solomon, M., Belenghi, B., Delledonne, M., Menachem, E., and Levine, A. (1999). The involvement of cysteine proteases and protease inhibitor genes in the regulation of programmed cell death in plants. Plant Cell **11:** 431–444.

Sorensen, A.M., Kröber, S., Unte, U.S., Huijser, P., Dekker, K., and Saedler, H. (2003). The Arabidopsis ABORTED MICROSPORES (AMS) gene encodes a MYC class transcription factor. Plant J. **33:** 413–423.

Strässer, K., Masuda, S., Mason, P., Pfannstiel, J., Oppizzi, M., Rodriguez-Navarro, S., Rondón, A.G., Aguilera, A., Struhl, K., Reed, R., and Hurt, E. (2002). TREX is a conserved complex coupling transcription with messenger RNA export. Nature **417:** 304–308.

Tanner, N.K., and Linder, P. (2001). DExD/H box RNA helicases: From qgeneric motors to specific dissociation functions. Mol. Cell **8:** 251–262.

Tewari, M., Yu, M., Ross, B., Dean, C., Giordano, A., and Rubin, R. (1997). AAC-11, a novel cDNA that inhibits apoptosis after growth factor withdrawal. Cancer Res. **57:** 4063–4069.

Van den Berghe, L., Laurell, H., Huez, I., Zanibellato, C., Prats, H., and Bugler, B. (2000). FIF [fibroblast growth factor-2 (FGF-2)-interacting-factor], a nuclear putatively antiapoptotic factor, interacts specifically with FGF-2. Mol. Endocrinol. **14:** 1709–1724.

Varnier, A.L., Mazeyrat-Gourbeyre, F., Sangwan, R.S., and Clément, C. (2005). Programmed cell death progressively models the development of anther sporophytic tissues from the tapetum and is triggered in pollen grains during maturation. J. Struct. Biol. **152:** 118–128.

Walter, M., Chaban, C., Schütze, K., Batistic, O., Weckermann, K., Näke, C., Blazevic, D., Grefen, C., Schumacher, K., Oecking, C., Harter, K., and Kudla, J. (2004). Visualization of protein interactions in living plant cells using bimolecular fluorescence complementation. Plant J. **40:** 428–438.

Wang, A., Xia, Q., Xie, W., Datla, R., and Selvaraj, G. (2003). The classical Ubisch bodies carry a sporophytically produced structural protein (RAFTIN) that is essential for pollen development. Proc. Natl. Acad. Sci. USA **100:** 14487–14492.

Wang, C., and Liu, Z. (2006). *Arabidopsis* ribonucleotide reductases are critical for cell cycle progression, DNA damage repair, and plant development. Plant Cell **18:** 350–365.

Wang, Y., Duby, G., Purnelle, B., and Boutry, M. (2000). Tobacco VDL gene encodes a plastid DEAD box RNA helicase and is involved in chloroplast differentiation and plant morphogenesis. Plant Cell **12:** 2129–2142.

Warthmann, N., Chen, H., Ossowski, S., Weigel, D., and Hervé, P. (2008). Highly specific gene silencing by artificial miRNAs in rice. PLoS One **3:** e1829.

Wilson, Z.A., and Zhang, D.B. (2009). From Arabidopsis to rice: Pathways in pollen development. J. Exp. Bot. **60:** 1479–1492.

Wu, C., Li, X., Yuan, W., Chen, G., Kilian, A., Li, J., Xu, C., Li, X., Zhou, D.X., Wang, S., and Zhang, Q. (2003). Development of enhancer trap lines for functional analysis of the rice genome. Plant J. **35:** 418–427.

Wu, H.M., and Cheung, A.Y. (2000). Programmed cell death in plant reproduction. Plant Mol. Biol. **44:** 267–281.

Xu, J., Yang, C., Yuan, Z., Zhang, D., Gondwe, M.Y., Ding, Z., Liang, W., Zhang, D., and Wilson, Z.A. (2010). The ABORTED MICROSPORES regulatory network is required for postmeiotic male reproductive development in *Arabidopsis thaliana*. Plant Cell **22:** 91–107.

Xue, W., Xing, Y., Weng, X., Zhao, Y., Tang, W., Wang, L., Zhou, H., Yu, S., Xu, C., Li, X., and Zhang, Q. (2008). Natural variation in *Ghd7* is an important regulator of heading date and yield potential in rice. Nat. Genet. **40:** 761–767.

Yang, C., Vizcay-Barrena, G., Conner, K., and Wilson, Z.A. (2007). MALE STERILITY1 is required for tapetal development and pollen wall biosynthesis. Plant Cell **19:** 3530–3548.

Zhang, D., Liang, W., Yin, C., Zong, J., Gu, F., and Zhang, D. (2010). OsC6, encoding a lipid transfer protein, is required for postmeiotic anther development in rice. Plant Physiol. **154:** 149–162.

Zhang, D.B., and Wilson, Z.A. (2009). Stamen specification and anther development in rice. Chin. Sci. Bull. **54:** 2342–2353.

Zhang, D.S., Liang, W.Q., Yuan, Z., Li, N., Shi, J., Wang, J., Liu, Y.M., Yu, W.J., and Zhang, D.B. (2008). Tapetum degeneration retardation is critical for aliphatic metabolism and gene regulation during rice pollen development. Mol. Plant **1:** 599–610.

Zhang, J., Li, C., Wu, C., Xiong, L., Chen, G., Zhang, Q., and Wang, S. (2006a). RMD: A rice mutant database for functional analysis of the rice genome. Nucleic Acids Res. **34** (Database issue): D745–D748.

Zhang, W., Sun, Y., Timofejeva, L., Chen, C., Grossniklaus, U., and Ma, H. (2006b). Regulation of Arabidopsis tapetum development and function by DYSFUNCTIONAL TAPETUM1 (DYT1) encoding a putative bHLH transcription factor. Development **133:** 3085–3095.